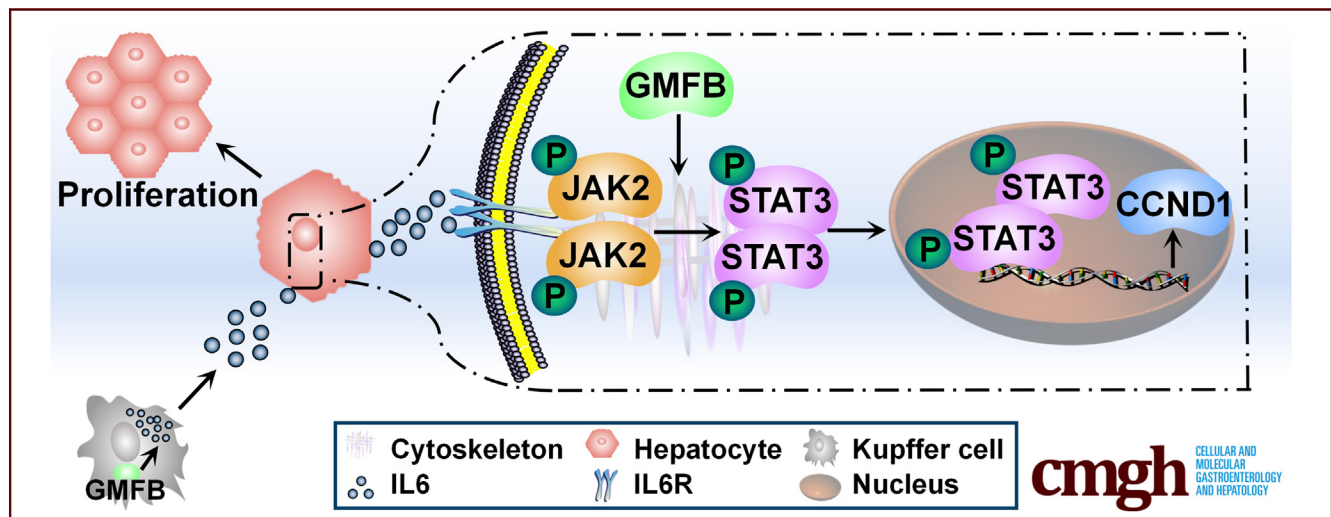


ORIGINAL RESEARCH

Glia Maturation Factor- β Supports Liver Regeneration by Remodeling Actin Network to Enhance STAT3 Proliferative Signals

Guo Yin,^{1,2,3,*} Weilan Zeng,^{1,3,*} Rong Li,⁴ Manman Zeng,⁵ Ronghua Chen,² Yaxue Liu,^{1,3} Ronglong Jiang,⁶ and Yan Wang^{1,6}

¹Biomedical Research Center, Southern Medical University, Guangzhou, China; ²Medical Research Center of Nanfang Hospital, Southern Medical University, Guangzhou, China; ³School of Pharmaceutical Science, Southern Medical University, Guangzhou, China; ⁴Department of Radiation Oncology, Affiliated Cancer Hospital & Institute of Guangzhou Medical University, Guangzhou, China; ⁵Department of Gynecology, Women and Children's Hospital of Guangdong, Guangzhou, China; and ⁶Department of Hepatology, Southern Medical University Affiliated Shenzhen Hospital, Shenzhen, China



SUMMARY

Glia maturation factor- β , an actin-remodeling factor, has shown important implications in liver diseases. We report on its role in liver pathophysiology. Glia maturation factor- β significantly supports liver regeneration after acute injury by promoting a proinflammatory microenvironment and hepatocyte proliferation.

BACKGROUND & AIMS: Glia maturation factor- β (GMFB) is a *bona fide* member of the actin depolymerizing factor homology family. Recently, emerging evidence suggested its implication in liver diseases, but data on its role in liver remain limited.

METHODS: Assessment of GMFB in liver histology, impact on liver regeneration and hepatocyte proliferation, and the underlying molecular pathways were conducted using mouse models with acute liver injury.

RESULTS: GMFB is widely distributed in normal liver. Its expression increases within 24 hours after partial hepatectomy (PHx). Adult *Gmfb* knockout mice and wild-type littermates are

similar in gross appearance, body weight, liver function, and histology. However, compared with wild-type control, *Gmfb* knockout mice post-PHx develop more serious liver damage and steatosis and have delayed liver regeneration; the dominant change in liver transcriptome at 24 hours after PHx is the significantly suppressed acute inflammation pathways; the top down-regulated gene sets relate to interleukin (IL)6/Janus kinase/signal transducer and activator of transcription 3 (STAT3) signaling. Another mouse model intoxicated with carbon tetrachloride replicated these findings. Furthermore, *Gmfb* knockout and wild-type groups have the similar numbers of Kupffer cells, but *Gmfb* knockout Kupffer cells once stimulated produce less IL6, tumor necrosis factor, and IL1 β . In hepatocytes treated with IL6, GMFB associates positively with cell proliferation and STAT3/cyclin D1 activation, but without any direct interaction with STAT3. In *Gmfb* knockout hepatocytes, cytoskeleton-related gene expression was changed significantly, with an abnormal-appearing morphology of actin networks. In hepatocyte modeling, actin-filament turnover, STAT3 activation, and metabolite excretion show a strong reliance on the status of actin-filament organization.

CONCLUSIONS: GMFB plays a significant role in liver regeneration by promoting acute inflammatory response in Kupffer cells and by intracellularly coordinating the responsive hepatocyte

proliferation. (*Cell Mol Gastroenterol Hepatol* 2022;14:1123–1145; <https://doi.org/10.1016/j.jcmgh.2022.07.016>)

Keywords: Glia Maturation Factor- β ; Acute Liver Injury; Inflammatory Response; Hepatocyte Proliferation.

Normal liver is characterized by a remarkable regeneration capacity. In response to diverse injuries or resection, quiescent hepatocytes can be triggered to regenerate and restore the original mass and function.^{1,2} Liver regeneration is a multistep and timely orchestrated process. A number of signaling molecules have been recognized regulating liver regeneration.^{3,4} After 2/3 partial hepatectomy (PHx), in the acute phase response, tumor necrosis factor (TNF) and interleukin (IL)1 β induce activation of nuclear factor- κ B (NF- κ B) and increase the release of IL6.^{5,6} When IL6 combines with its membrane receptor, signal transducer and activator of transcription 3 (STAT3) becomes phosphorylated at tyrosine 705 (Y705) by receptor-associated Janus kinase (JAK). The phospho-STAT3 (p-STAT3) enters into the nucleus after dimerization and binds to the cyclin D1 promoter. Then, the hepatocyte proliferation begins.^{7,8}

Glia maturation factor (GMF) is a *bona fide* member of the actin depolymerizing factor homology family conserved from yeast to mammals.⁹ Glia maturation factor- β (GMFB), a GMF isoform, has specific activity in regulating the spatial organization of actin filaments. GMFB binds to actin-related protein 2/3 complex to remodel branched actin-filaments networks, thus underpinning cell motility and endocytic trafficking.^{10,11} Meanwhile, there also is collective evidence indicating that GMFB is related to brain development and its response to various stresses.^{12–14} GMFB facilitates the secretion of proinflammatory factors in microglia cells in the brain, and its silencing can block the activation of inflammatory pathways such as p38 mitogen-activated protein kinase and NF- κ B.^{13,14} GMFB also has been identified in the human liver proteome.^{15,16} The level of GMFB in early stage hepatocellular carcinoma (HCC) has been shown to be significantly higher than that in the surrounding non-HCC liver tissue,¹⁶ and, in a very recent study, it even shows significant correlation with HCC prognosis.¹⁷ However, data on the particular role of GMFB in the liver remain very limited.

Given these developments, in this study we aimed to determine the histologic distribution of GMFB in the liver, its associated cellular function, and the possible molecular pathways in the process of liver regeneration after acute damage by using mouse models. We hypothesized that GMFB could be involved positively in liver regeneration.

Results

GMFB Is Expressed Physiologically in Liver Cells and Its Expression Increases With Liver Regeneration After PHx

We first assessed the presence of GMFB in the normal liver of C57BL/6 mice. GMFB was found to be widely


distributed in the liver and relatively more in the cytoplasm of liver cells (Figure 1A). After 2/3 PHx, the level of GMFB in the remnant liver had a marked increase starting at 6 hours and peaking at 48 hours compared with the baseline level (Figure 1B). We then co-stained liver sections with anti-GMFB, anti-Hepatocyte nuclear factor 4 α (HNF4 α , hepatocyte marker), anti-F4/80 (Kupffer cell marker), and anti-desmin (hepatic stellate cell marker) antibodies, hepatocytes, and Kupffer cells, but not hepatic stellate cells (HSCs), are clearly discernible for the positive staining of GMFB (Figure 1C). Because HSCs appear too small in the liver section images to be clearly examined for their GMFB staining, we isolated these cells and observed them *in vitro*. The HSCs were shown to be GMFB-positive either at their quiescent state (3 days after seeding) or their activated state (21 days after seeding) (Figure 2). In addition, we explored several clinical databases containing liver transcriptome or proteome, and found that GMFB expression was increased in liver of HCC or in those with chronic hepatitis, but was reduced in liver with acute failure compared with normal controls (Figure 3).^{16,18–21} These data also imply a positive correlation between liver cell proliferation and GMFB expression.

GMFB Deficiency Has Delayed Liver Regeneration After PHx

To determine the effect of GMFB on liver regeneration, we constructed a *Gmfb* knockout (KO) C57BL/6 mouse line by clustered regularly interspaced short palindromic repeats (CRISPR)-CRISPR-associated (Cas) system 9 (CRISPR-Cas9). *Gmfb* KO was confirmed by Western blot (Figure 1D), quantitative real-time polymerase chain reaction (qPCR) (Figure 1D), and immunofluorescence assays (Figure 1E). *Gmfb* KO mice and wild-type (WT) littermates are similar in terms of appearance, gross behavior, general health, and body weight. Furthermore, neither H&E staining nor ultrastructural microscopy showed any obvious differences in liver sections between the 2 groups (Figure 1E). A hepatic biochemical panel including alanine aminotransferase,

*Authors share co-first authorship.

Abbreviations used in this paper: BC, bile canaliculi; CCl₄, carbon tetrachloride; CDK, cyclin-dependent kinase; CMFDA, 5-chloromethylfluorescein diacetate; DAPI, 4',6-diamidino-2-phenylindole; DMEM, Dulbecco's modified Eagle medium; EdU, 5-ethynyl-2'-deoxyuridine; FBS, fetal bovine serum; FITC, fluorescein isothiocyanate; GMF, glia maturation factor; GMFB, glia maturation factor β ; gRNA, guide RNA; HCC, hepatocellular carcinoma; HNF4 α , hepatocyte nuclear factor 4 α ; HSC, hepatic stellate cell; IL, interleukin; JAK, Janus kinase; KO, knockout; LPS, lipopolysaccharide; MKI67, marker of proliferation Ki-67; NF- κ B, nuclear factor kappa B; OI, object of interest; PBS, phosphate-buffered saline; p-STAT3, phosphorylated signal transducer and activator of transcription 3; p-YAP, phosphorylated yes-associated protein 1; PHx, partial hepatectomy; qPCR, quantitative real-time polymerase chain reaction; RNA-seq, RNA sequencing; siRNA, small interfering RNA; STAT3, signal transducer and activator of transcription 3; TNF, tumor necrosis factor α ; WT, wild-type; YAP1, yes-associated protein 1; Y705, tyrosine 705.

 Most current article

© 2022 The Authors. Published by Elsevier Inc. on behalf of the AGA Institute. This is an open access article under the CC BY-NC-ND license (<http://creativecommons.org/licenses/by-nc-nd/4.0/>).

2352-345X

<https://doi.org/10.1016/j.jcmgh.2022.07.016>

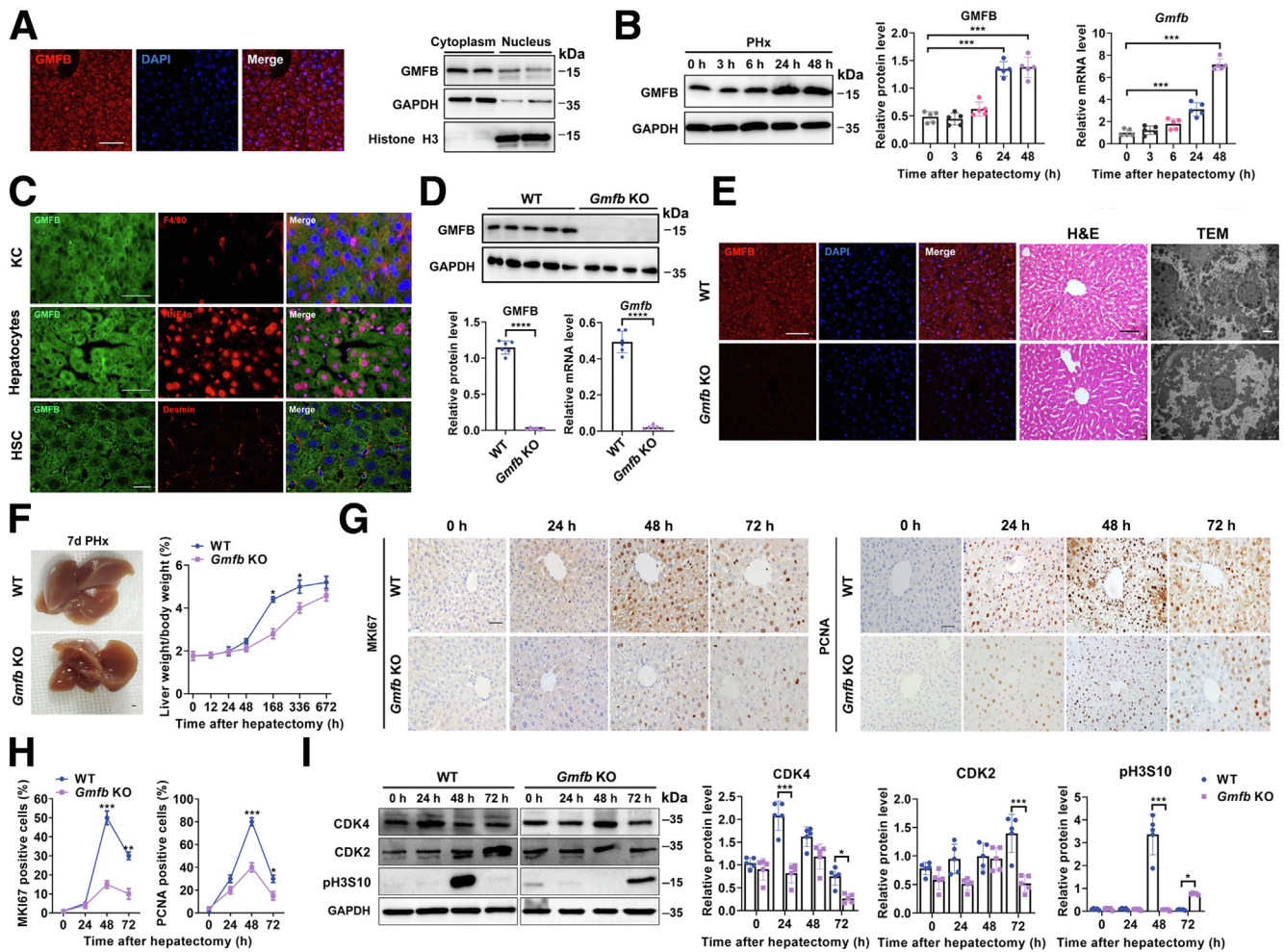


Figure 1. GMFB expression is related positively to liver regeneration in mice after PHx. (A) Representative immunofluorescent images showing distribution of GMFB (anti-GMFB, red) in normal liver tissues from WT mice and GMFB protein expression in cytoplasm and nucleus of liver cells. $n = 5$ mice for each group. Scale bar: $50 \mu\text{m}$. (B) Expression levels of GMFB protein and messenger RNA (mRNA) in liver of WT mice at the indicated time points after PHx. $n = 5$ mice for each group. One-way analysis of variance, $*P < .05$, $***P < .001$, vs 0 hours after PHx. (C) Representative immunofluorescent images in liver tissue slices from WT mice after PHx showing distribution of GMFB (anti-GMFB, green) in Kupffer cells (anti-F4/80, red), hepatocytes (anti-HNF4 α , red), and HSCs (antidesmin, red). Scale bar: $50 \mu\text{m}$. (D) Expression levels of GMFB protein and mRNA in liver from *Gmfb* KO and WT mice. $n = 6$ mice for each group. Two-tailed t test, $****P < .0001$, vs WT controls. (E) Representative immunofluorescent (anti-GMFB, red; DAPI, blue; scale bar: $50 \mu\text{m}$), H&E staining (scale bar: $50 \mu\text{m}$), and transmission electron microscopy (TEM) (scale bar: $2 \mu\text{m}$) images in slices of liver tissue from *Gmfb* KO and WT mice. (F) Remnant liver volume from *Gmfb* KO and WT mice at 7 days after PHx (scale bar: 1mm) and liver-to-body weight ratio at the indicated time points after PHx. $n = 4$ mice for each group. Two-tailed t test, $*P < .05$, vs WT controls. (G) Representative immunohistochemical images in anti-MKI67 (brown) and anti-proliferating cell nuclear antigen (PCNA)-stained (brown) liver sections from *Gmfb* KO and WT groups. Scale bar: $50 \mu\text{m}$. (H) Quantification of MKI67 and PCNA-positive staining cells in liver slices from *Gmfb* KO and WT groups. $n = 4$ mice for each group. Two-tailed t test, $*P < .05$, $**P < .01$, and $***P < .001$, vs WT controls. (I) Expression levels of CDK4, CDK2, and histone H3 serine 10 phosphorylation (pHS10) proteins in liver from *Gmfb* KO and WT mice at the indicated time points after PHx. $n = 5$ mice for each group. Two-tailed t test, $*P < .05$, $**P < .01$, and $***P < .001$, vs WT controls. Data represent the average of 3 independent experiments. GAPDH, glyceraldehyde-3-phosphate dehydrogenase; KC, Kupffer cell.

aspartate aminotransferase, total bilirubin, and alkaline phosphatase also showed no differences between the 2 groups.

Then, *Gmfb* KO and WT mice were subjected to PHx. At 6 hours after PHx, both groups start to drink water and slight movement and have no mortality before being killed.

Normally, the liver-to-body weight ratio in rodents will re-establish to original levels within 5–7 days after PHx.²² However, compared with WT controls, *Gmfb* KO mice recovered with a smaller volume of remnant liver, showing the significantly lower liver-to-body weight ratio after 7 days post-PHx (Figure 1F). Nonetheless, at 28 days after

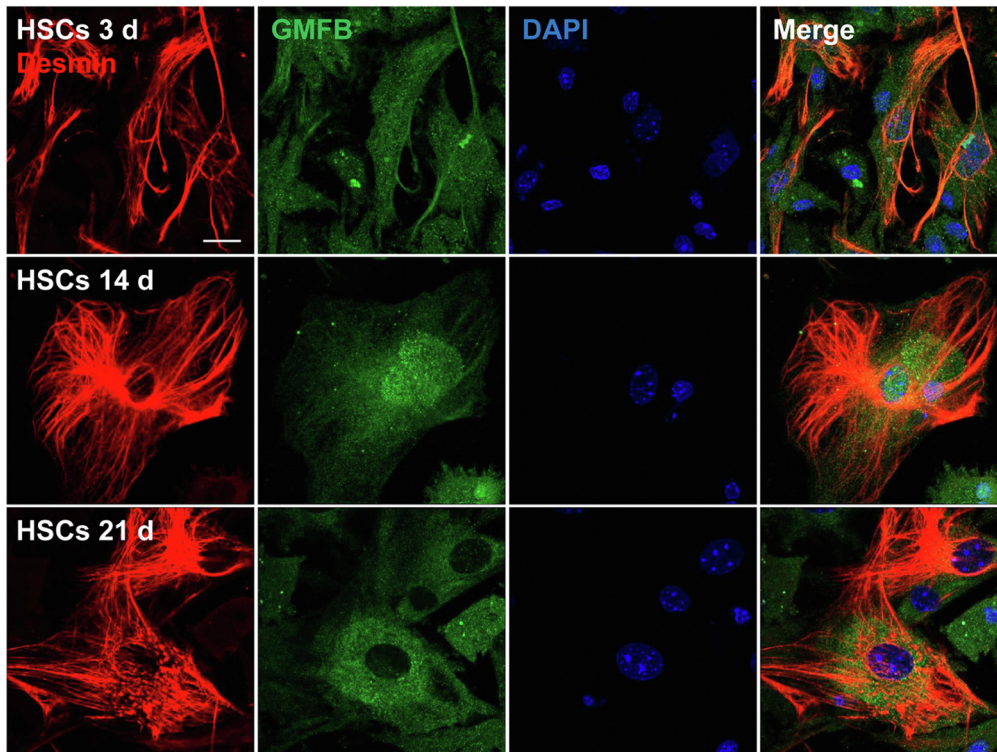


Figure 2. Presence of GMFB in HSCs isolated from WT mice. Representative immunofluorescent images showing the presence of GMFB (anti-GMFB, green) and desmin (anti-desmin, red) in primary HSCs at 3, 14, and 21 days after seeding. Scale bar: 20 μm . Data represent the average of 3 independent experiments.

PHx the liver volume and liver-to-body weight ratio in KO mice was comparable with WT controls (Figure 1F). Further examination of liver histology and hepatocyte size, including average cell size and range of cell size, showed that these KO mice at 28 days after PHx seem to have higher numbers of large hepatocytes than the WT controls, but without any statistical significance (Figure 4). Even though the final liver regeneration was not abrogated, it does not imply the specific signaling pathway is not important, because rapid liver regeneration or not can make the difference between life or death in clinical practice.³

We further observed the liver regeneration status in these mice. Liver histologic examination showed the significantly less proportions of positive staining of marker of proliferation Ki-67 (MKI67) (marker for all phases of the cell cycle) and proliferating cell nuclear antigen (marker for DNA synthesis) in *Gmfb* KO mice at 48 and 72 hours after PHx compared with WT controls (Figure 1G and H). Figure 1I further shows that G1 (cyclin-dependent kinase [CDK]4), G1-S (CDK2), and mitosis (histone H3 serine 10 phosphorylation) phases of the cell cycle may have been perturbed in *Gmfb* KO liver. Altogether, these data suggest that *Gmfb* KO is associated with a slower liver regeneration after PHx.

Gmfb KO Liver Has Greater Hepatocyte Injury and More Enhanced Hepatic Steatosis After PHx

Compared with WT control, *Gmfb* KO mice after PHx have more vacuolated hepatocytes (Figure 5A). From 12 to 48 hours after PHx, the serum levels of the hepatic

biochemical panel in the *Gmfb* KO mice are approximately 1- to 5-fold higher than in WT control (Figure 5B). These results suggest that GMFB deficiency could be associated with greater injury in hepatocytes and more impaired hepatic function.

Normally, in hepatocytes a significant accumulation of lipids will appear from 1 to 3 days after PHx.²³ However, compared with WT control, *Gmfb* KO mice show a significantly greater extent of liver steatosis and higher levels of serum cholesterol and triglycerides from 12 to 48 hours after PHx (Figure 5C and D). Such a difference also was shown in the oleic acid cultured primary hepatocytes isolated from *Gmfb* KO and WT mice (Figure 5E). We then assessed the functional genes related to lipid and glucose turnover in the liver samples. Figure 5F shows that, in terms of cellular input, synthesis, metabolism, output of lipids and glucose, and the formation of lipid droplets, *Gmfb* KO and WT groups have a similar gene expression levels at 0 hours (baseline); and at 24 hours after PHx, in the *Gmfb* KO group only *Acc1* (2.39 times higher; $P < .01$), *Gpam* (1.51 times higher; $P = .011$), and *Ppar α* (0.59 times lower; $P = .012$) had levels that were different from their WT controls at 24 hours (Figure 6A). However, these differences were nonsignificant at their protein levels (Figure 6B).

These data altogether show that most functional pathways underlying lipid turnover in hepatocytes of *Gmfb* KO mice could be relatively as normal as the WT control. Moreover, considering the basic molecular role of GMFB as a *bona fide* component in actin binding, we reasoned that the

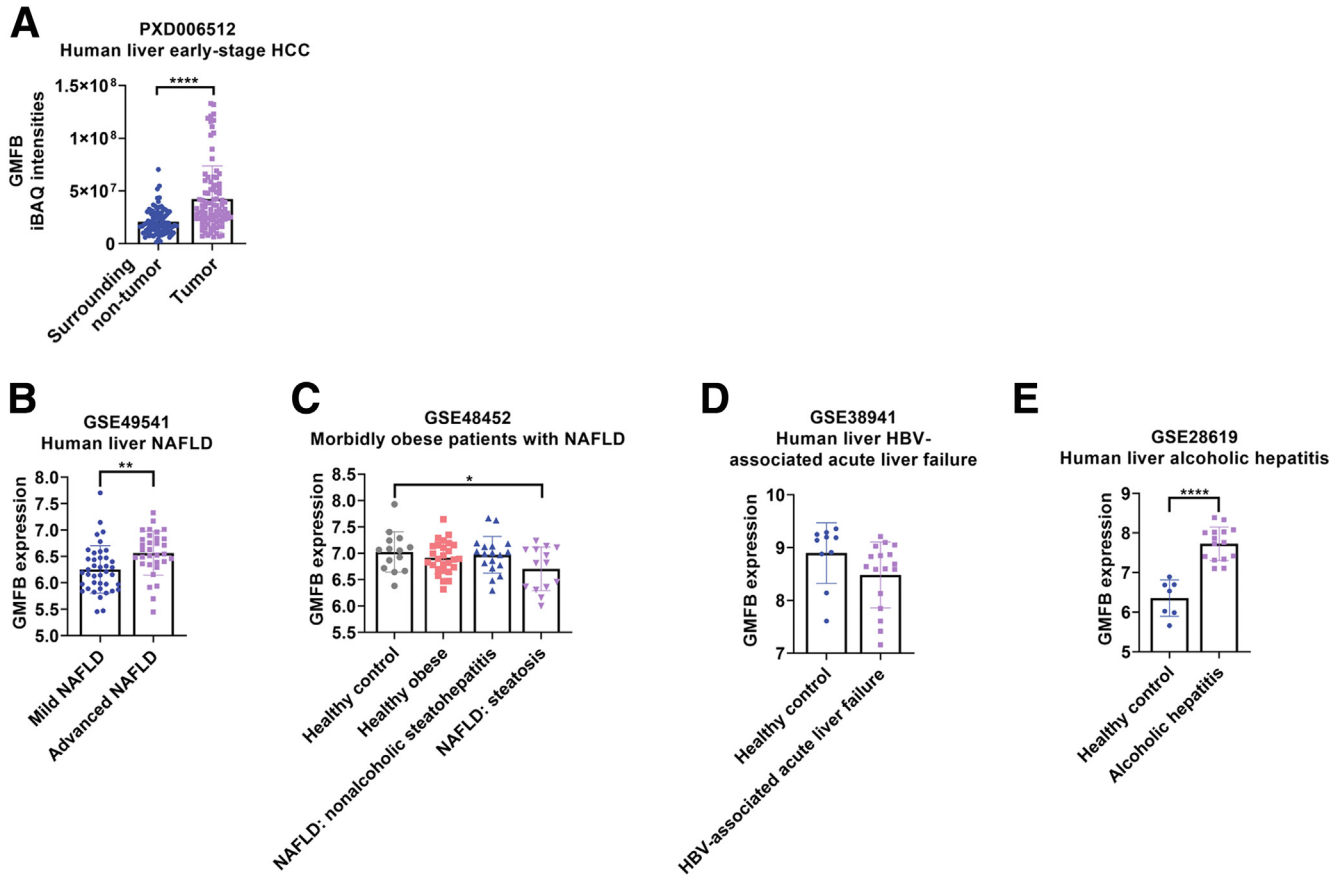


Figure 3. Expression levels of GMFB protein (proteome) and messenger RNA (transcriptome) in liver from chronic liver disease and control groups in published clinical databases. (A) Proteomic data from database published by Jiang et al.¹⁶ N = 110 paired liver tissues with chronic hepatitis B virus (HBV) infection. Two-tailed *t* test, *****P* < .0001. (B–E) Transcriptomic data from databases published by Moylan et al.¹⁸ (B) N = 40 mild stage, 32 advanced-stage liver samples from nonalcoholic fatty liver disease (NAFLD) patients. Two-tailed *t* test, ***P* < .01, as published by Ahrens et al.¹⁹ (C) N = 14 healthy controls, 27 healthy obese, 18 nonalcoholic steatohepatitis, and 14 steatosis liver samples. One-way analysis of variance, **P* < .05, as published by Nissim et al.²⁰ (D) N = 10 healthy controls and 17 HBV-associated acute liver failure liver samples. Two-tailed *t* test, as published by Affò et al.²¹ (E) N = 7 healthy controls and 15 alcoholic hepatitis liver samples. Two-tailed *t* test, *****P* < .0001.

higher accumulation of lipid droplets in hepatocytes with GMFB deficiency might be driven in part by the impaired cytoskeleton-transport route within the cells, which needs further investigation.

Acute Inflammatory Pathways Generally Are Attenuated in *Gmfb* KO Liver After PHx

We further analyzed the transcriptome of remnant liver in *Gmfb* KO mice using RNA sequencing (RNA-seq). At 0-hour baseline, compared with WT control, the *Gmfb* KO group has 259 up-regulated genes and 631 down-regulated genes (Figures 5G and 7A); the major differences from WT control are the up-regulation of hepatic metabolism of fatty acids and xenobiotics and the down-regulation of the inflammatory response (Figures 5H and 7E, Supplementary Tables 1 and 2). At 24 hours after PHx, compared with 0-hour baseline, the major changes in the WT group are down-regulation of 1227 genes involving mainly metabolism processes related to xenobiotic and lipid metabolism,

and up-regulation of 759 genes involving mainly acute inflammatory response, acute-phase response, and cell migration processes (Figures 5G and I, 7B and F, and Supplementary Tables 1 and 2), which overall are the typical functional shifts in liver regeneration after PHx.³ Compared with 0-hour baseline, the *Gmfb* KO group at 24 hours after PHx had a similar ratio of up-regulated to down-regulated genes to the WT controls (Figures 5G and 7B and C); but the major changes in the *Gmfb* KO group were the down-regulation of metabolic processes related mainly to amino acids and small molecules, and up-regulation of ribosome biogenesis and nucleoside biosynthetic processes (Figures 5J and 7G, and Supplementary Tables 1 and 2), which is very different from the WT controls. At 24 hours after PHx, compared with WT control, the *Gmfb* KO group showed a dominant down-regulation of cellular response to innate immune activating stimulus, and the up-regulation of processes related mainly to DNA replication (Figures 5K, and 7D and H, and Supplementary Tables 1 and 2). Noting that most processes of cell inflammatory response, such as

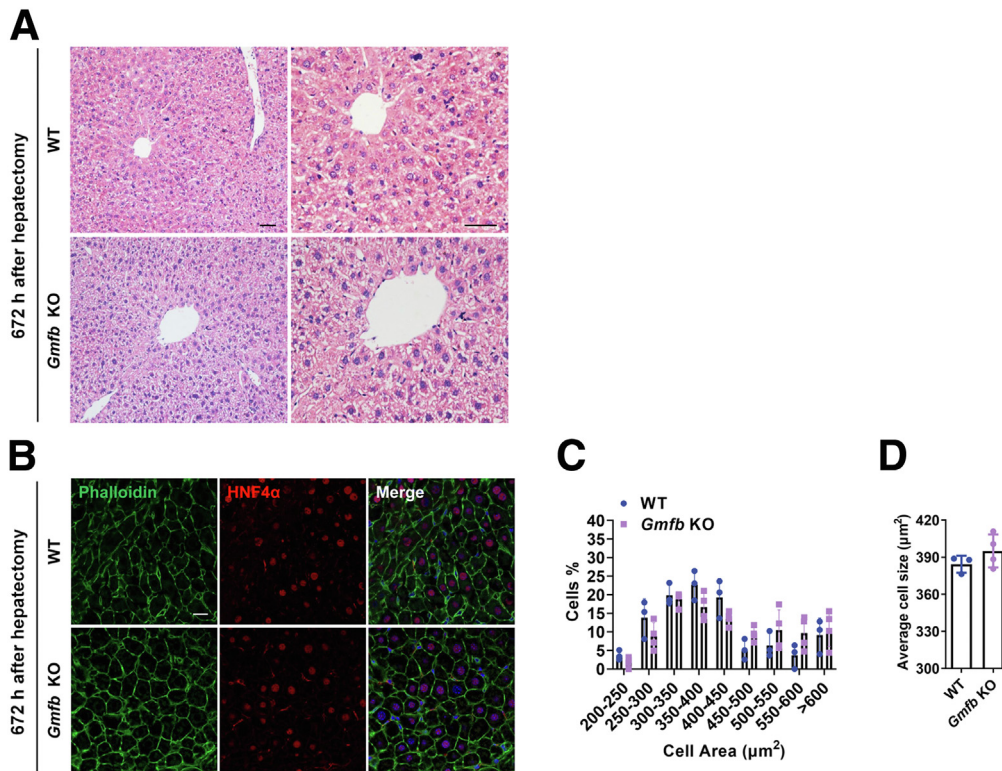


Figure 4. Histologic assessment of hepatocytes in liver from mice at 672 hours after PHx. (A) Representative H&E staining images in liver slices from the indicated mice groups. Scale bar: 50 μm . $n = 3-4$ mice for each group. (B-D) Representative immunofluorescent images in phalloidin (green) and anti-HNF4 α (red)-stained liver cryosections from the indicated mice groups (scale bar: 20 μm), and quantification of the proportion of HNF4 α -positive staining cells with different sizes and the average cell size of HNF4 α -positive staining cells in these slices. $n = 3-4$ mice for each group. Two-tailed t test, vs WT controls.

TNF, Toll-like receptor, NF- κ B, mitogen-activated protein kinase signaling pathways, and related functions such as cytokine binding and activity, chemokine receptor binding and activity overwhelmingly are down-regulated (Supplementary Tables 1 and 2), so the acute inflammatory response in *Gmfb* KO liver after PHx could be impaired substantially. Furthermore, because their liver cells have no obvious deficiency in the functional process of DNA replication, the delayed liver regeneration in *Gmfb* KO mice could be associated mainly with the deficient inflammatory response in liver.

IL6/JAK/STAT3/Cyclin D1 Axis and Proinflammatory Microenvironment in *Gmfb* KO Liver After PHx Are Suppressed Significantly

We further identified the gene sets related to the suppressed functional processes in liver regeneration in *Gmfb* KO vs WT groups. On gene set enrichment analysis, the top one gene set with the most statistical significance was related to IL6/JAK/STAT3 signaling (Figure 8A and B), for which most genes in the *Gmfb* KO group at 24 hours after PHx had lower levels of expression than their WT controls (Figure 8C). Interestingly, in the *Gmfb* KO groups, expression levels of these genes at 24 hours after PHx were similar to or even lower than their own expression levels at 0-hour baseline (Figure 8C). Thus, IL6/JAK/STAT3 signaling in the acute inflammatory response to PHx seems likely to be generally inhibited in *Gmfb* KO liver.

In the acute inflammatory response during liver regeneration after PHx, inflammatory cytokines such as IL6, TNF,

and IL1 β play an important role in orchestrating the intracellular pathways for cell proliferation and cell-cell interaction.⁴ We further determined, as shown in Figure 8D, that the expressions of IL6, TNF, and IL1 β all are up-regulated in the remnant liver of WT mice from 3 to 24 hours after PHx, noting that IL6 shows a dramatically increased expression as early as 3 hours and increases up to a 5-fold higher expression level at 48 hours than its baseline level, which is important for the initiation and maintenance of the regeneration process³; but in the *Gmfb* KO group, as anticipated, the up-regulation of these cytokines has been attenuated overall. IL6 directly promotes liver cell proliferation and protection and is a key cytokine in liver regeneration after PHx.^{4,24} The remnant liver in *Gmfb* KO mice also shows a lower level of IL6-positive staining than the WT control (Figure 8E).

The major pathway that mediates the effect of IL6 on liver proliferation after acute injury is the JAK/STAT3/cyclin D1 cascade.²⁵⁻²⁷ STAT3 is phosphorylated by the IL6-receptor-associated activated JAK and translocated to cell nucleus and then mediates the transcription of target genes such as cyclin D1. In the *Gmfb* KO group, the levels of phospho-JAK2 (p-JAK2) and p-STAT3 (Y705) both are significantly lower than those in WT controls from 3 hours to the proliferation peak 48 hours after PHx (Figure 8F). The level of cyclin D1 is decreased significantly in an accordant way (Figure 8F). These data not only confirmed the earlier-described transcriptome findings about the suppressed IL6/JAK/STAT3 signaling, but also partly explain the impaired proliferation of liver cells.

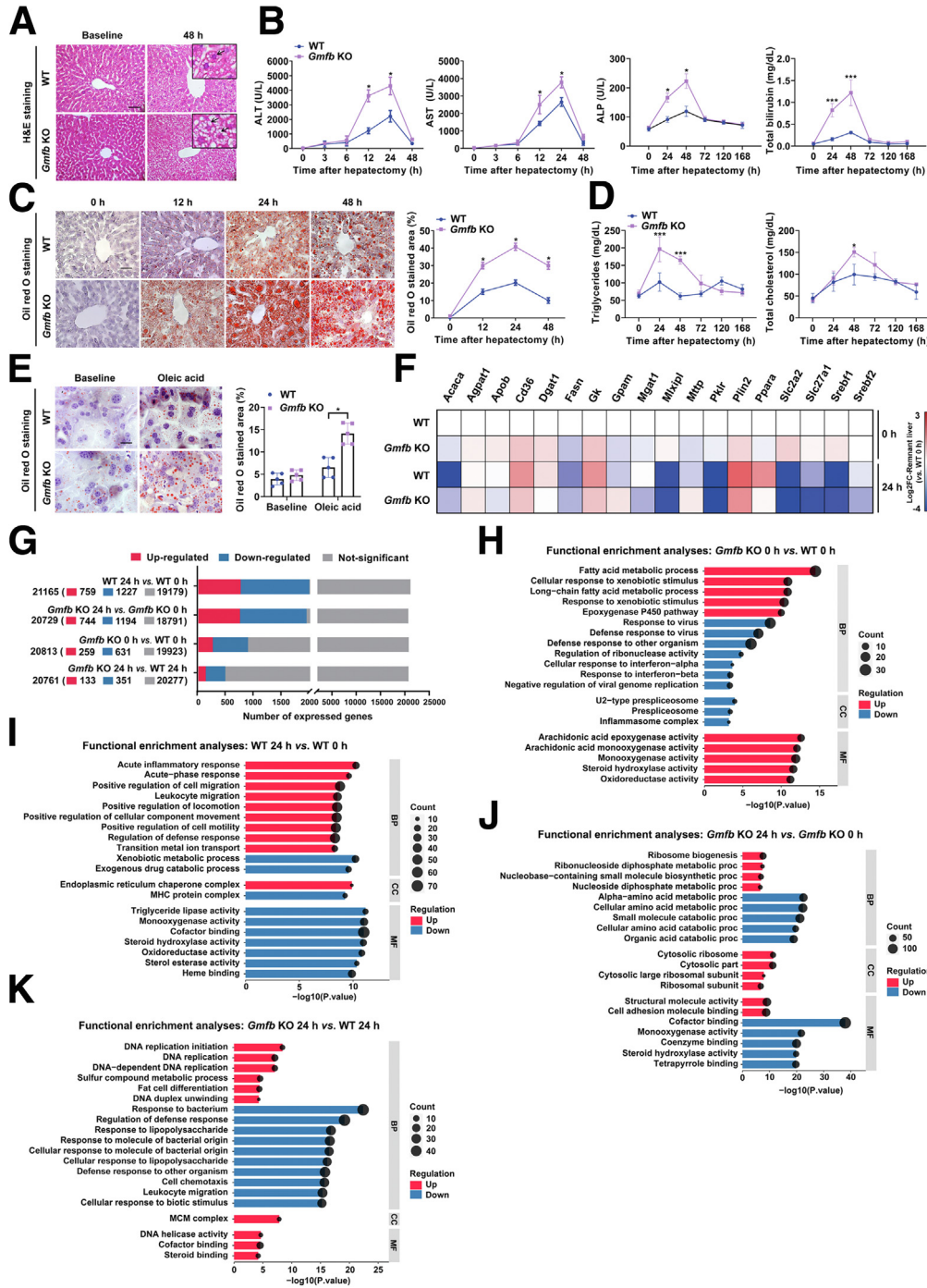


Figure 5. Liver tissue injury and transcriptomics profiling in *Gmfb* KO mice after PHx. (A) Representative H&E staining images in liver slices from indicated mice. Black arrows indicate vacuolated hepatocytes. Scale bar: 50 μ m. (B) Serum levels of alanine aminotransferase (ALT), aspartate aminotransferase (AST), alkaline phosphatase (ALP), and total bilirubin at the indicated time points. *n* = 4 mice for each group. Two-tailed *t* test, $*P < .05$, $***P < .001$, vs WT controls. (C) Representative oil red O staining (red) images in liver slices (scale bar: 50 μ m) and the percentage of positive staining area. *n* = 5 mice for each group. Two-tailed *t* test, $*P < .05$, vs WT controls. (D) Serum levels of triglyceride and total cholesterol at the indicated time points. *n* = 4 mice for each group. Two-tailed *t* test, $*P < .05$, $***P < .001$, vs WT controls. (E) Representative oil red O staining (red) images in primary hepatocytes cultured with oleic acid and the percentage of positive staining cells. *n* > 100 cells for each group. Two-tailed *t* test, $*P < 0.05$, vs WT control. (F) log₂ fold change in gene expression (qPCR) in liver from *Gmfb* KO and WT mice (vs WT 0 hours) for the indicated genes. *n* = 5–6 mice for each group. (G) Bar plot showing the numbers of expressed genes with significantly up-regulated or down-regulated or nonsignificant change in expression level (RNA-seq) for the indicated comparison groups. *n* = 2 mice for each group. (H–K) Functional enrichment analyses using Gene Ontology pathways for the significantly up- and down-expressed genes (RNA-seq) in comparison with (H) *Gmfb* KO 0 hours vs WT 0 hours; (I) WT 24 hours vs WT 0 hours; (J) *Gmfb* KO 24 hours vs *Gmfb* KO 0 hours; (K) *Gmfb* KO 24 hours vs WT 24 hours. *n* = 2 mice for each group. BP, biological process; CC, cellular component; MF, molecular function.

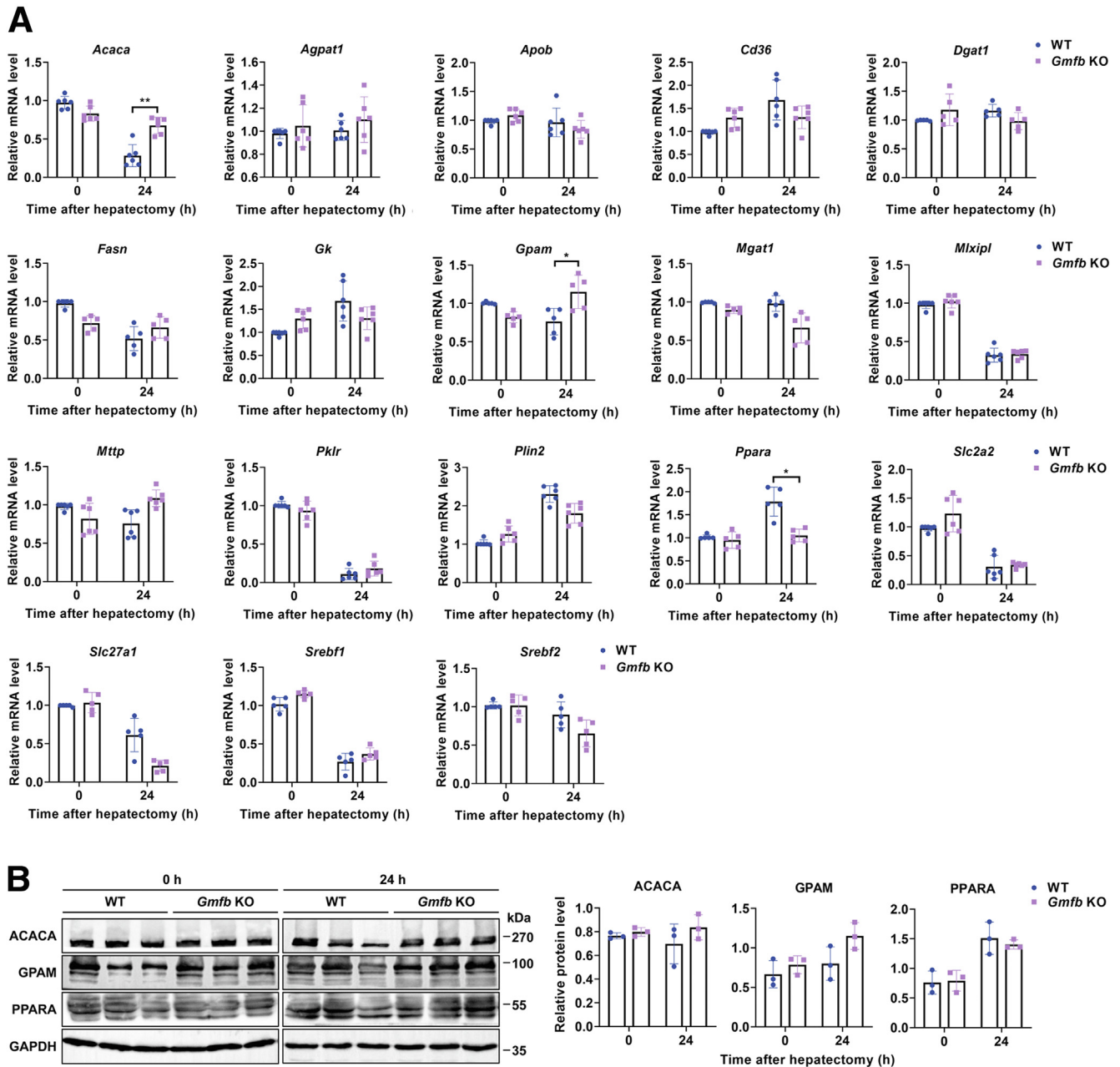


Figure 6. Expression levels of indicated genes and proteins in liver from *Gmfb* KO and WT mice after PHx. (A) Expression levels of indicated genes by qPCR. (B) Expression levels of indicated proteins that have significant changes in gene expression in the test performed in panel A. $n = 5-6$ mice for qPCR or 3 mice for Western blot for each group. Two-tailed t test, $*P < .05$, $**P < .01$, vs WT controls. ACACA, acetyl-coenzyme A carboxylase α ; GAPDH, glyceraldehyde-3-phosphate dehydrogenase; GPAM, glycerol-3-phosphate acyltransferase, mitochondrial; PPARA, peroxisome proliferator activated receptor α .

Kupffer cells are a major source of liver cells responsible for producing inflammatory cytokines, including IL6, TNF, and IL1 β , thus playing a critical role in establishing the microenvironment of innate immune response to PHx.^{28,29} Because Kupffer cells physiologically express GMFB in our detection, we determined the inflammatory response of Kupffer cells to PHx. First, on immunofluorescence imaging analysis, we found similar numbers of F4/80-positive cells in

WT and *Gmfb* KO groups at 24 hours after PHx (Figure 8G). Then, we isolated primary Kupffer cells from *Gmfb* KO and WT mice and stimulated them with lipopolysaccharide (LPS). We witnessed significantly less production of IL6, TNF, and IL1 β by the *Gmfb* KO Kupffer cells compared with their WT controls (Figure 8H). Thus, the subnormal proinflammatory microenvironment in *Gmfb* KO liver after PHx partly results from the weakened response of Kupffer cells.

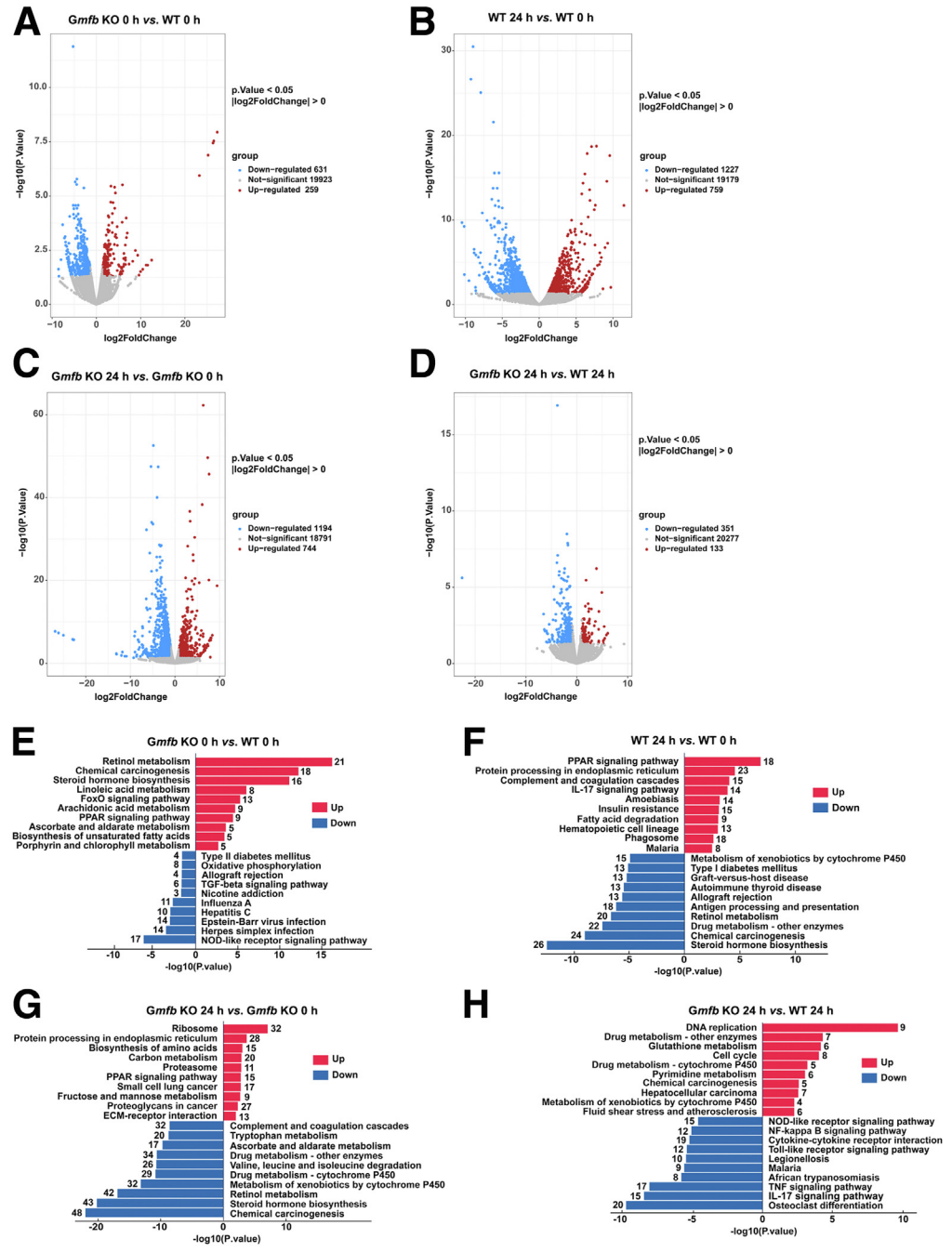


Figure 7. Differentially expressed (A–D) gene and (E–H) KEGG analyses of transcriptome data (RNA-seq) for liver samples from *Gmfb* KO and WT mice after PHx. N = 2 mice for each group. KEGG, Kyoto Encyclopedia of Genes and Genomes. ECM, extracellular matrix; FoxO, forkhead box O; NOD, nucleotide-binding oligomerization domain; PPAR, peroxisome proliferator activated receptor.

Gmfb After Mice Have Impaired Liver Regeneration With Deficient Acute Inflammatory Response After Carbon Tetrachloride-Induced Acute Liver Injury

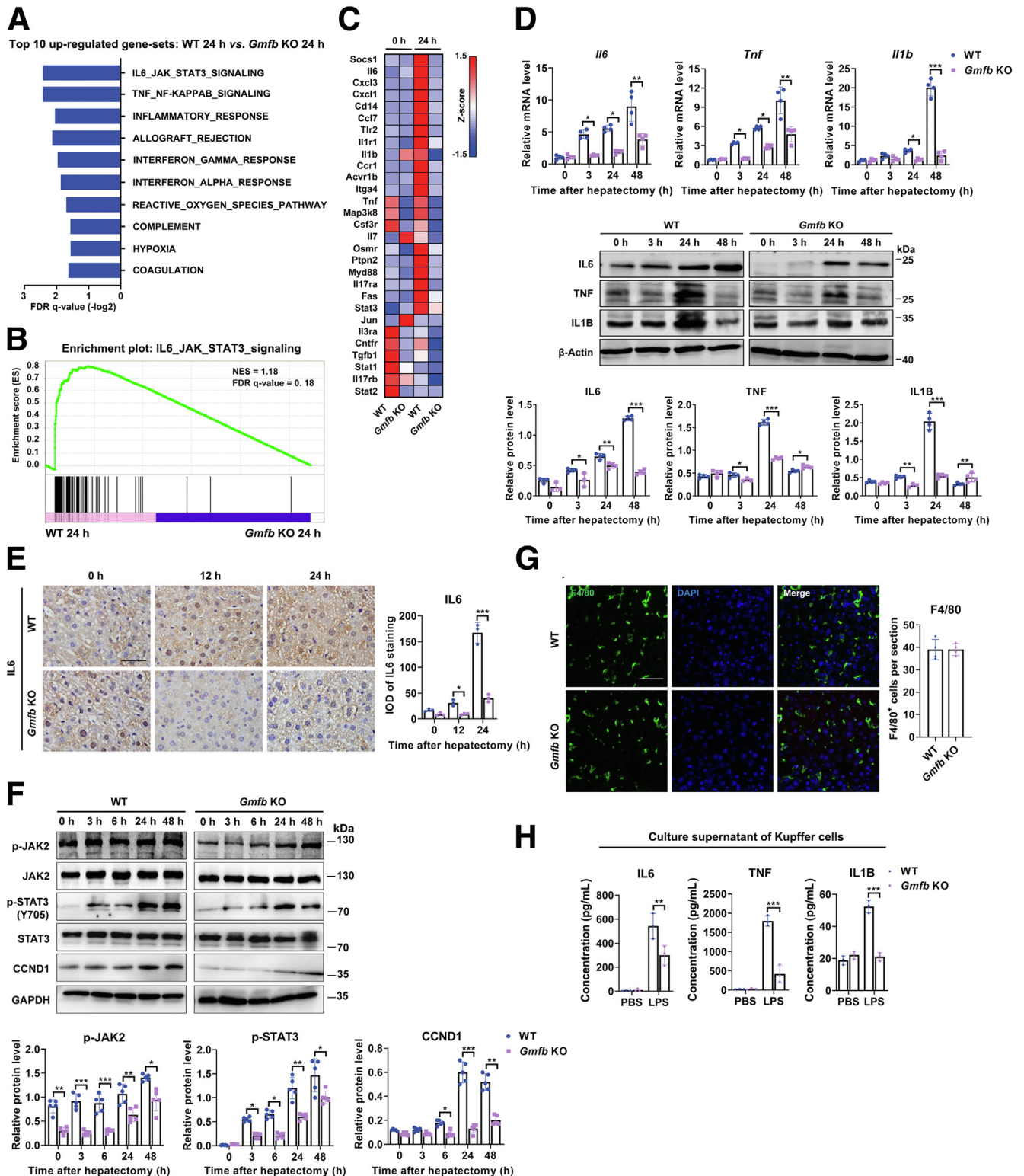
One-dose administration of carbon tetrachloride (CCl₄) is commonly used in the study of liver regeneration in response to an acute toxic injury. Compared with WT control, *Gmfb* KO mice with CCl₄ injection have decreased liver cell proliferation, showing a significantly lower proportion of MKI67-positive staining (Figure 9A); and have enhanced liver injury, showing significantly higher levels of serum

alanine aminotransferase and aspartate aminotransferase (Figure 9B), a larger area of liver necrosis (Figure 9C), and a greater extent of hepatic steatosis (Figure 9D) from 24 to 72 hours after injection. Furthermore, the activation level of STAT3/cyclin D1 and up-regulation of *Il6*, *Tnf*, and *Il1β* were attenuated overall (Figure 9E and F) in the *Gmfb* KO group compared with WT controls. These results are consistent with those found in the PHx model, suggesting that GMFB also is associated with liver regeneration in CCl₄-induced acute liver injury, partly by engaging the signaling of the acute inflammatory response.

GMFB Associates Positively With Hepatocyte Proliferation and STAT3 Activation in Response to IL6 Treatment

We further analyzed whether GMFB could have any direct effect on cell proliferation and activation of STAT3 signaling in hepatocytes. First, *GMFB* knockdown and overexpression were modeled in L02 cells, a human

hepatocyte cell line, by small interfering RNA (siRNA) or plasmid transfection, respectively (Figure 10A and B). We found no differences between the cells with *GMFB* knock-down or overexpression and their controls in terms of the level of cell proliferation (Figure 11A and B), distribution of cell-cycle phases (Figure 11C and D), and activation level of the STAT3/cyclin D1 axis (Figure 11E and F). These data are



not unexpected because *Gmfb* KO and WT mice have a comparable status of cell proliferation in their livers under normal conditions (as indicated by data at 0 hours in Figure 1F–J).

Then, we treated the transfected cells with IL6 (15 ng/mL) to model the *in vivo* condition of stress. We found that the level of cell proliferation (Figures 10C and D, and 11G and H), distribution of cell-cycle phases (Figure 10E and F), activation level of the STAT3/cyclin D1 axis (Figure 10G and H), and the proportion of nucleus translocation of STAT3 (Figure 10I and J) all become positively associated with the level of GMFB expression in these cells. To further determine whether GMFB directly could interact with STAT3, we performed co-immunoprecipitation analysis of L02 cells under IL6 treatment, showing that there is no direct interaction between them (Figure 11J). These data are intriguing because they show that GMFB in hepatocytes cannot directly activate the STAT3/cyclin D1 axis but rather takes part in some process that substantially facilitates the activation of the STAT3/cyclin D1 axis.

Moreover, we challenged the PHx mice with an immediate subsequent injection of LPS to enhance inflammatory stress in the resected liver. The levels of p-STAT3 and cyclin D1 in the livers of *Gmfb* KO mice with PHx + LPS (Figure 11J) appear to be a little higher than those in the livers of *Gmfb* KO mice with only PHx (Figure 8F) for up to 6 hours after surgery; but they persist to be significantly lower than their WT controls through 24 hours of observation (Figure 11J). These data provide more evidence to support the fact that GMFB has a significant and positive impact on cell proliferation signaling in the liver after acute injury.

Gmfb KO-Related Abnormal Organization of Actin Cytoskeleton Contributes to the Inefficient Activation of STAT3 in Hepatocytes

Proper activation of STAT3 requires normal organization of cytoskeleton in cells.^{30,31} GMFB catalyzes the debranching of the actin-filament network, and is essential to normal cytoskeleton organization.⁹ We report the effect of GMFB on

hepatocyte cytoskeleton. Therefore, we first observed the actin-filament organization in the cultured primary hepatocytes isolated from *Gmfb* KO and WT mice. At 72 hours after seeding, in WT hepatocytes, actin filaments appear long and straight, and the collecting bunches form some beam/sector-like structures (Figure 12A, A'); whereas in *Gmfb* KO hepatocytes, actin filaments appear short and diverse in their direction, and form some irregular honeycomb-like structures (Figure 12A, A'). The apparently increased branching of actin filaments might be owing to the deficiency of GMFB function (debranching). We then compared the cytoskeleton-related gene sets in liver samples, *Gmfb* KO and WT groups have remarkably different patterns of gene expression at 0-hour baseline and at 24 hours after PHx (Figure 12B).

Then, to determine whether STAT3 activation is associated with actin-filament organization in hepatocytes, we treated primary hepatocytes at 48 hours after seeding with latrunculin B (2 μ g/mL) to disrupt their actin networks, and with IL6 to activate STAT3 signaling as illustrated in Figure 12C; we detected the actin-network morphology and level of STAT3 activation in cells at 3 phases, defined by the status of actin-filament organization (Figure 12C): phase 1, baseline of actin-filament organization under normal conditions without latrunculin B treatment; phase 2, depolymerization of actin filaments with latrunculin B treatment; and phase 3, repolymerization of actin filaments with latrunculin B washed off. On imaging analysis, at phase 1 *Gmfb* KO and WT hepatocytes show the different appearances of actin networks (Figure 12D), as we have observed (Figure 12A). At phase 2, the appearances of actin-filament depolymerization resulting from latrunculin B treatment in *Gmfb* KO and WT hepatocytes are comparable, both showing a significant absence of actin filaments in cytosol and the cell boundary (Figure 12D). At phase 3, 2 hours after washing off latrunculin B, in comparison with WT hepatocytes, *Gmfb* KO hepatocytes show a remarkably lower level of actin filaments along their cell boundary and within their cytosol (Figure 12D), indicating that the recovery of actin-filament organization in *Gmfb* KO hepatocytes has been delayed. In

Figure 8. (See previous page). **The IL6/JAK2/STAT3/cyclin D1 pathway of acute inflammation response to PHx is suppressed significantly in *Gmfb* KO mice.** (A) Rank using gene set enrichment analysis (GSEA) for the up-expressed gene sets (RNA-seq) associated with comparison of WT 24 hours vs *Gmfb* KO 24 hours after PHx. Of the top 10 gene sets of enrichment, the top 5 have statistical significance (defined by INESI > 1, FDR q value < 0.25). n = 2 mice for each group. (B) GSEA plot showing an enrichment of the differently expressed gene sets (RNA-seq) associated with IL6-JAK-STAT3 signaling in comparison with WT 24 hours vs *Gmfb* KO 24 hours after PHx. n = 2 mice for each group. (C) Heatmap showing the gene expression values (fragments per kilobase of transcript per million mapped reads) of indicated genes (RNA-seq) associated with IL6-JAK-STAT3 signaling in comparison with WT and *Gmfb* KO groups. n = 2 mice for each group. (D) Expression levels of IL6, TNF, and IL1 β messenger RNA and their proteins in liver from mice groups at the indicated time points after PHx. n = 4 mice for each group. Two-tailed *t* test, **P* < .05, ****P* < .001, vs WT controls. (E) Representative immunohistochemical images in liver sections showing IL6 (anti-IL6, brown) distribution and quantification of IL6-positive staining density. Scale bar: 50 μ m. n = 3 mice for each group. Two-tailed *t* test, **P* < .05, ****P* < .001, vs WT controls. (F) Expression levels of p-JAK2, JAK2, p-STAT3, STAT3, and CCND1 proteins in liver from *Gmfb* KO and WT mice at the indicated time points after PHx. n = 5 mice for each group. Two-tailed *t* test, **P* < .05, ***P* < .01, and ****P* < .001, vs WT controls. (G) Representative immunofluorescent images in liver sections from *Gmfb* KO and WT mice after PHx showing Kupffer cell (anti-F4/80, green; DAPI, blue) distribution and quantification of positive cell numbers per section. Scale bar: 50 μ m. n = 4 mice for each group. Two-tailed *t* test. (H) Concentrations of IL6, TNF, and IL1 β in culture supernatant of Kupffer cells treated with 20 μ g/mL LPS or control. Two-tailed *t* test, ***P* < .01, ****P* < .001, vs WT controls. Data represent the average of 3 independent experiments. CCND1, cyclin D1; FDR, false-discovery rate; GAPDH, glyceraldehyde-3-phosphate dehydrogenase; IOD, integrated optical density; NES, normalized enrichment score.

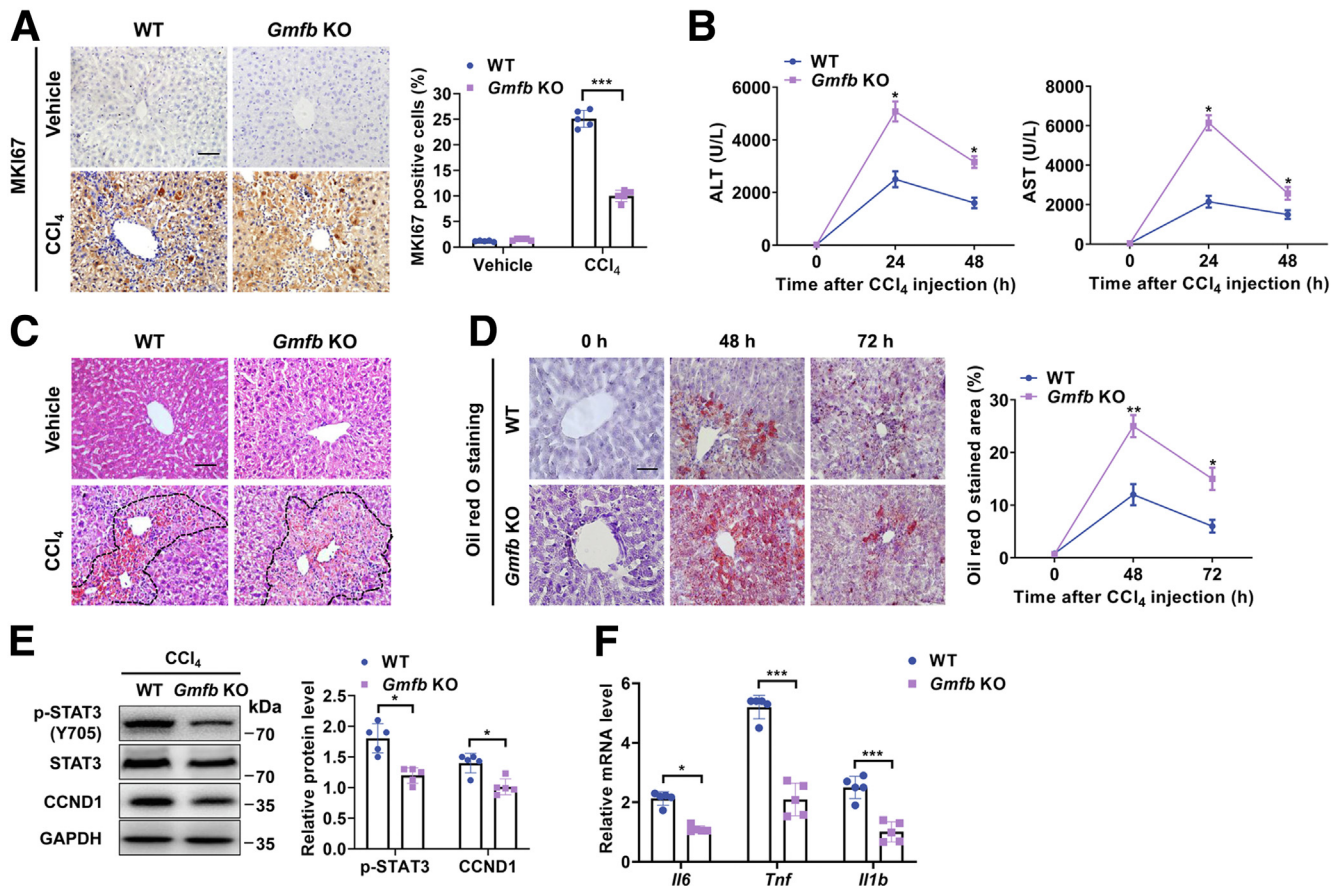


Figure 9. *Gmfb* KO mice have impaired liver regeneration after CCl₄-induced acute liver injury. (A) Representative immunochemical images in anti-MKI67– (brown) stained liver sections from *Gmfb* KO and WT groups (scale bar: 50 μ m) and quantification of positive staining cells. $n = 5$ mice for each group. Two-tailed t test, $***P < .001$, vs WT controls. (B) Serum levels of alanine aminotransferase (ALT) and aspartate aminotransferase (AST) in *Gmfb* KO and WT groups. $n = 5$ mice for each group. Two-tailed t test, $*P < .05$, vs WT controls. (C) Representative H&E staining images in liver sections from *Gmfb* KO and WT groups (scale bar: 50 μ m). Liver necrosis is indicated by the area surrounded by the black dashed line. (D) Representative oil red O staining (red) images in liver sections from *Gmfb* KO and WT groups (scale bar: 50 μ m) and the percentage of positive staining area. $n = 4$ mice for each group. Two-tailed t test, $*P < .05$, $**P < .01$, vs WT controls. (E) Protein levels of p-STAT3, STAT3, and CCND1 in liver from *Gmfb* KO and WT groups. $n = 5$ mice for each group. Two-tailed t test, $*P < .05$, vs WT controls. (F) Levels of *Il6*, *Tnf*, and *Il1b* messenger RNA in liver from *Gmfb* KO and WT groups. $n = 5$ mice for each group. Two-tailed t test, $***P < .001$, vs WT controls. CCND1, cyclin D1; GAPDH, glyceraldehyde-3-phosphate dehydrogenase.

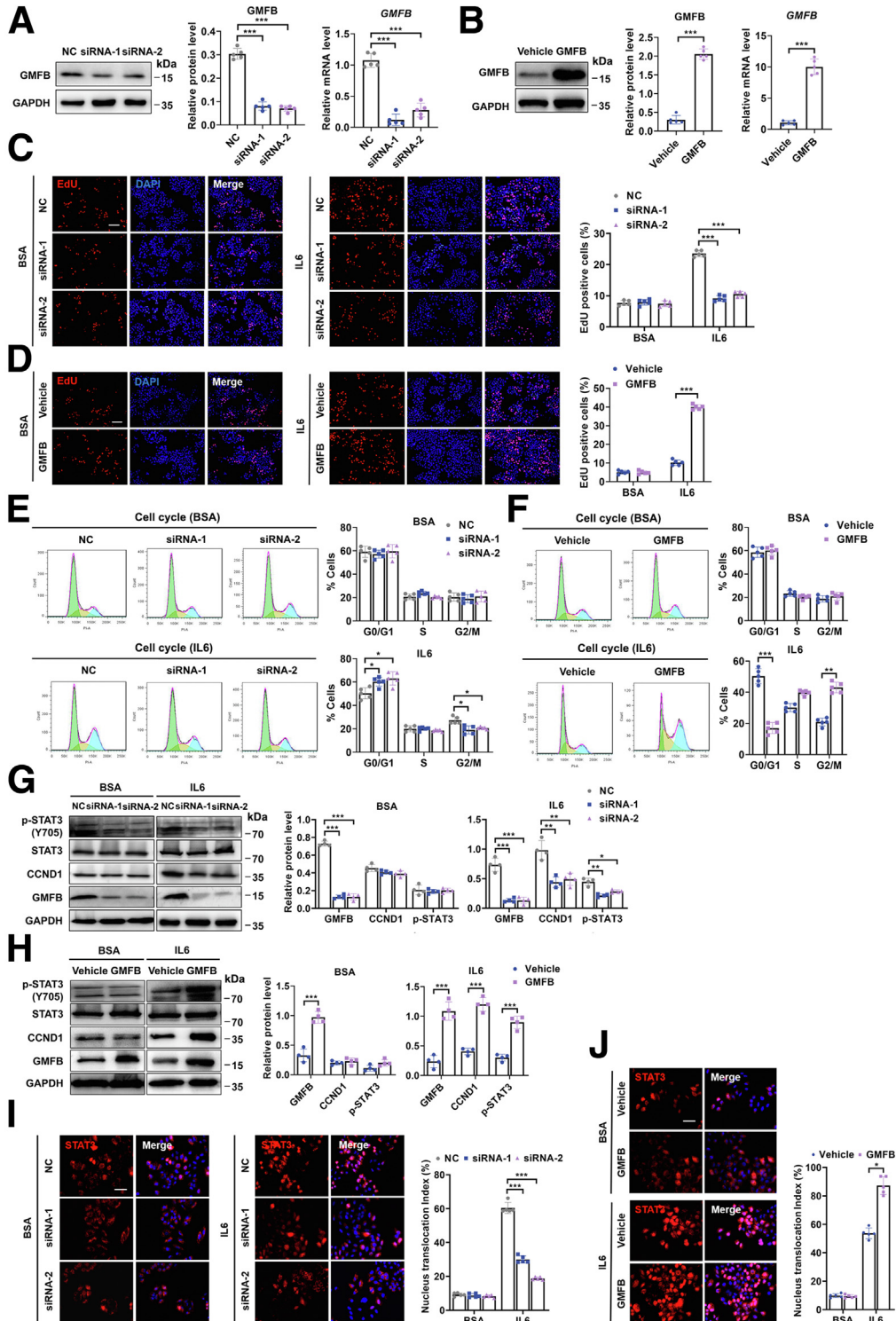
the meantime, in both groups, STAT3 activation by IL6 stimulation is almost completely blocked at phase 2 when actin-filament organization is seriously disrupted (Figure 12E), and largely is recovered at phase 3 when actin networks recover (Figure 12E). Moreover, the level of STAT3 activation is comparable between the 2 groups at phase 2, but it still was significantly lower in *Gmfb* KO hepatocytes than in WT hepatocytes at phase 3, as it was at phase 1 (Figure 12E), for which both the trend and extent in the differences were consistent with the image results. Thus, the status of STAT3 activation is in close concordance with the status of actin-filament organization. Altogether, these results provide strong evidence that, in hepatocytes, the organization status of actin filaments has substantial influence on the status of STAT3 activation in response to IL6 stimulation. Thus, GMFB deficiency, which directly causes abnormal organization of actin filaments, can impair the response of STAT3 activation.

Gmfb KO-Related Abnormal Organization of Actin Cytoskeleton Also Leads to Dysfunctioning of Hepatic Excretion Through Bile Canaliculi

Actin filaments beneath the plasma membrane are essential elements that compose the structure of bile canaliculi (BC) between adjacent hepatocytes. BC formation and function often are considered the surrogate marker for hepatic metabolism and metabolite excretion. Thus, we investigated further whether the altered actin-filament organization associated with *Gmfb* KO could have any effect on BC formation and function. We found that at 24 hours after seeding the alignment of actin filaments on the junction borders between adjacent WT hepatocytes appear tight, linear, and continuous (Figure 12F, F'), whereas those between adjacent *Gmfb* KO hepatocytes seem loose, twisted, and intermittent (Figure 12F, F''). We further determined the process of excretion of 5-chloromethyl-fluorescein

diacetate (CMFDA) from hepatocytes into BC.³² CMFDA has significantly more accumulation in the cytosol of *Gmfb* KO hepatocytes (Figure 12G). Moreover, by using super-resolution microscopy, we detected significantly less excretion of CMFDA between adjacent *Gmfb* KO hepatocytes (Figure 12G, G') compared with WT hepatocytes (Figure 12G, G'). Overall, these data suggest that hepatocytes in

Gmfb KO mice may have actin-filament organization-related cellular dysfunction, such as disrupted excretion of hepatic metabolites during regeneration. In light of this, given that no significant change occurred to the metabolic pathways for lipid droplet turnover in the liver of *Gmfb* KO mice after PHx, the more enhanced hepatic steatosis could be attributed in part to the abnormal actin networks in hepatocytes.



GMFB Deficiency Does Not Decrease Yes-Associated Protein 1 Activation in Liver Regeneration After PHx

The role of yes-associated protein 1 (YAP) activation in liver regeneration after PHx and its regulation by biomechanical inputs increasingly have been recognized.³³ GMFB shows an obvious effect on the organization of actin filaments in hepatocytes; we then determined if there could be any change in YAP activation in regeneration of the *Gmfb* KO liver. The levels of YAP and phosphorylated-YAP (p-YAP) (S127) in whole liver tissue both increase significantly from 0 to 24 hours after PHx, but have no significant differences between the WT and *Gmfb* KO groups (Figure 13A). Moreover, in cytosol isolated from the liver tissue, the level of p-YAP from 0 to 24 hours has no significant difference between WT and *Gmfb* KO mice, and for both mice groups there is no significant difference in the p-YAP level between the 2 time points; while in the nucleus, the level of YAP increases significantly from 0 to 24 hours in both mice groups and the expression level in KO mice is significantly higher than that in WT mice at 24 hours (Figure 13B). We also found a higher ratio of YAP-positive staining nuclei in live tissue sections of KO mice than in WT mice at 24 hours after PHx, but the ratios at baseline, 72 hours, and 28 days after PHx were comparable between the mice groups (Figure 13C). Overall, these preliminary data imply that, compared with the condition of WT liver, YAP activation has not been down-regulated in the post-PHx liver regeneration with GMFB deficiency.

Discussion

Proper regeneration of hepatocytes is vital to prevent liver failure or mortality. This study shows that GMFB has a significant and positive impact on hepatic regeneration after acute injury by promoting a proinflammatory microenvironment and the responsive hepatocyte proliferation.

GMFB is conserved from yeast to mammals and expressed in diverse organs and tissues.^{9,34} We detected the physiological expression of GMFB in liver and found its expression increased significantly after PHx. The presence of GMFB was shown to be necessary for liver restoration on

time, alleviation of hepatocytes damage, and prevention of oversteatosis in the liver after acute injury. Thus, GMFB has a significant liver-protective role in the process of regenerative response to acute injury.

Adequate up-regulation of acute inflammation is essential for proper initiation of liver regeneration after acute injury.^{4,35} GMFB deficiency leads to an overall suppression of acute inflammatory pathways in the liver after PHx, which seems concordant with its inflammation-inducing activity observed in the previous neuroinflammatory disease studies.^{13,14} Noting that *Gmfb* is unconditionally knocked out in the present model, we have no idea what the status of the systemic immune response would be in these mice and what effect the systemic immune response can have on liver regeneration. Nonetheless, liver is well regarded as an organ with a self-constrained immune microenvironment. A priority can be made of the analysis of its local immune reaction. Among regenerative signaling, STAT3 is an acute-phase response factor functioning as a key signal transducer and transcription activator responsible for injury-induced liver regeneration; the IL6/JAK/STAT3 pathway has a major role in activating the STAT3/cyclin D1 axis in hepatocytes.^{8,24,36} The overall lower expression of acute inflammatory cytokines than normal controls can significantly undermine the activation of the JAK/STAT3/cyclin D1 axis in *Gmfb* KO liver, thus resulting in inadequate hepatocyte proliferation.

We identified GMFB physiologically localized in both Kupffer cells, hepatocytes, and HSCs. *Gmfb* KO has no obvious impact on the number of mature Kupffer cells (F4/80 positive) after PHx, but is associated with a significant decrease in the production of IL6, TNF, and IL1 β by these cells. Detailed mechanisms on how *Gmfb* KO has perturbed the function of Kupffer cells needs further exploration. Nonetheless, it is rational to speculate that the alleviated acute inflammatory microenvironment in the *Gmfb* KO liver after injury can be owing in part to the weakened response of Kupffer cells. We next tested the effect on activation of the STAT3/cyclin D1 axis in hepatocytes. We found that the GMFB effect can be limited only to the reaction of the axis rather than directly to the axis itself. Indeed, we did not detect any physically direct interaction between GMFB and

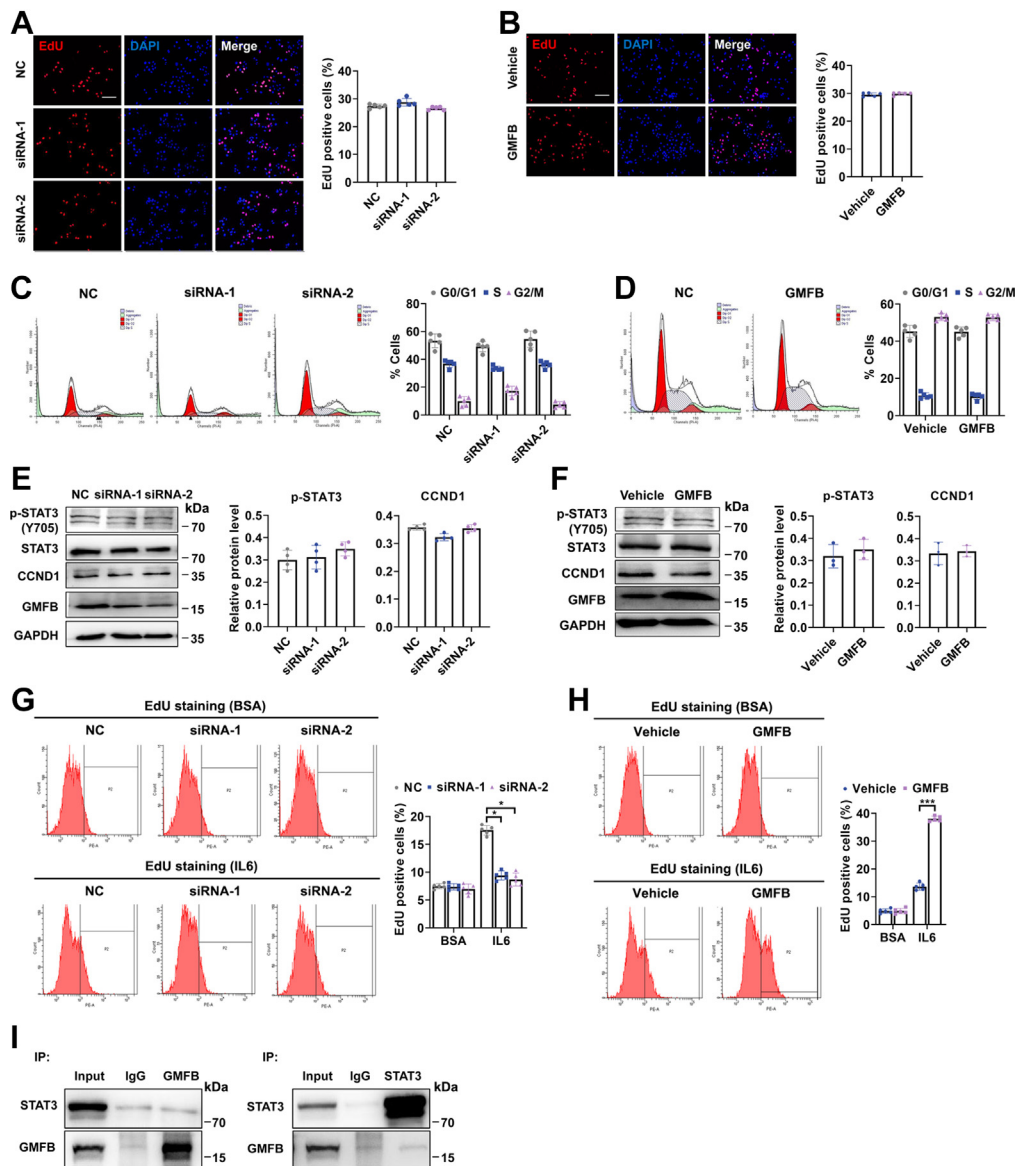
Figure 10. GMFB in hepatocytes positively associates with cell proliferation and STAT3 activation in cellular response to IL6 treatment. (A) Levels of GMFB protein and messenger RNA (mRNA) in L02 cells (hepatocyte cell line) transfected with GMFB siRNAs or control siRNA (normal control). One-way analysis of variance, $***P < .001$, vs NC group. (B) Levels of GMFB protein and mRNA in L02 cells transfected with GMFB overexpression plasmid (GMFB) or control plasmid (vehicle). Two-tailed t test, $***P < .001$, vs vehicle group. (C and D) Representative immunofluorescence staining images in transfected L02 cells stained with EdU (red) and DAPI (blue) with treatment of IL6 or bovine serum albumin (BSA) (scale bars: 100 μ m) and percentage of EdU-positive-staining cells. $n > 300$ cells for each group. (C) One-way analysis of variance, (D) 2-tailed t test, $***P < .001$, vs NC or vehicle groups. (E and F) Flow cytometry analyses showing the percentage of cells at cell-cycle phases G0/G1, S, or G2/M of transfected L02 cells with treatment of IL6 or BSA. $n > 10^6$ cells for each group. (E) One-way analysis of variance; (F) 2-tailed t test, $*P < .05$, $**P < .01$, and $***P < .001$, vs NC or vehicle groups. (G and H) Protein levels of GMFB, CCND1, p-STAT3, and STAT3 in transfected L02 cells with treatment of IL6 or BSA. (G) One-way analysis of variance; (H) 2-tailed t test, $*P < .05$, $**P < .01$, and $***P < .001$, vs NC or vehicle groups. (I and J) Representative immunofluorescence staining images in transfected L02 cells under IL6 or BSA treatment and stained with anti-STAT3 (red) and DAPI (blue) (scale bars: 50 μ m). The percentage of STAT3 nucleus translocation cells (STAT3 and DAPI overlay-positive staining). $n = 300$ cells for each group. (I) One-way analysis of variance; (J) 2-tailed t test, $*P < .05$, $***P < .001$, vs NC or vehicle groups. Data represent the average of 3 independent experiments. CCND1, cyclin D1; GAPDH, glyceraldehyde-3-phosphate dehydrogenase.

STAT3 signaling. This also was confirmed by the database information from BioGRID^{4,4} (<https://thebiogrid.org/109026> or 203523), showing that STAT3 and GMFB do not belong to interactor lists of each other. The expression of GMFB in HSCs was shown in the list of complementary DNA microarray data in 2 previous studies.^{37,38} Our study provides direct evidence showing the presence of GMFB in HSCs. The role of GMFB in HSC function in liver regeneration could be valuable, and warrants detailed assessment in a future investigation.³⁹

Recent mechanistic studies have identified the specific roles of GMFB in actin cytoskeleton remodeling.^{10,11} All of these discoveries seem to be inconsistent with its early assignment as a cell maturation factor in the brain.⁹ Consistent with previous data on GMFB and actin-filament organization, our data show a strong interdependent relationship between expression of GMFB, status of actin-filament organization, and activation of STAT3 signaling. The relationship can well interpret all other results found in our experiments,

and thus could be the basic mechanism for pathophysiological changes in the present model. Therefore, in some sense our study can be of important value for addressing the initiative on reconciliation of the actin functions of GMFs with their roles in signaling and disease.⁹ However, the step-by-step molecular mechanism underlying these effects still is unclear. Interestingly, although STAT3 activation can be significantly inhibited in the setting of GMFB deficiency-related cytoskeleton remodeling, the signaling of YAP activation seems not to have been negatively affected by this. YAP activation in liver cells can have many regulation factors such as cell polarity and adhesion, biomechanical signals, bile acids, and some nuclear receptors.³³ Our study has not provided any evidence clue showing how YAP activation is maintained in liver regeneration under GMFB deficiency, which, however, might partly explain the robustness in liver mass restoration of our animal model.

Our experiments were performed under the basic speculation that the involvement of the GMFB molecule is within



the cells. We did not perform any experiments to exclude the possibilities of any functional secretion of GMFB from liver cells, or of any extracellular involvement of GMFB in promoting liver regeneration. There was a study that showed GMFB among the up-regulated proteins listed in a proteomic analysis of the secretome of cultured non-parenchymal liver cells isolated from phenobarbital-treated rats,⁴⁰ but this study did not perform any additional protein tests or biochemical function experiments to validate the data. We haven't found any other data following this study. Moreover, the receptor to GMFs on the cell membrane still have not been found since the initial identification of GMF more than 40 years ago.¹² Despite this, because GMFB shows significant involvement in liver regeneration, further observations are needed to clarify all of these details.

In summary, our study shows that GMFB plays an active role in the process of liver regeneration after acute injury. On one hand, GMFB is involved in modulating the production of inflammatory cytokines in Kupffer cells and thus is necessary for establishing an adequate proinflammatory microenvironment. On the other hand, GMFB positively mediates the proliferative reaction of STAT3 activation by directly remodeling actin-filament organization in hepatocytes. Therefore, GMFB can serve as a potential target in future investigations on promoting liver regeneration and functional recovery after acute injury.

Methods

Reagent or Resource

The source and identifier for all the key reagents and resources are listed in [Supplementary Table 3](#).

Animals and Treatment

All animal experimental protocols were approved by the Ethical Committee for Animal Research of Southern Medical University (Guangzhou, China) and were conducted based on the state guidelines from the Ministry of Science and Technology of China. WT or *Gmfb* KO *C57BL/6* male mice at 8–10 weeks age were used in this study. The WT *C57BL/6* mice were purchased from the Laboratory Animal Center of Guangdong Province. The *Gmfb*^{-/-} *C57BL/6* mouse line was

constructed by the CRISPR–Cas9 system. The guide RNA (gRNA)1 targeted a 5'-GTTAGAGTGAAGCTTATATTAGG-3' sequence, the gRNA2 targeted a 5'-AAAACCTAAGCATGC-CAGGTGTGG-3' sequence, the gRNA3 targeted a 5'-CCGATTGTCTTAGTCACTTGAGG-3' sequence, and the gRNA4 targeted a 5'-TCTTAGTCACTTGAGGAGTGAGG-3' sequence, in the second exon of the *GMFB* gene. Genomic DNA of *GMFB* mutant mice were determined using PCR amplification of tail DNA. The primer sequences are listed in [Supplementary Table 4](#). The *gmfb* KO was confirmed by nucleic acid electrophoresis or gene sequencing. The genomic DNA of the *Gmfb* mutant mice was knocked out successfully by 509 bases. All animals were maintained in a climate-controlled environment (22°C–24°C and constant humidity 50%–70%) under a 12-hour light/dark cycle. All animals had ad libitum access to standard food and fresh water.

Mice Models of PHx, CCl₄ Intoxication, and LPS Stimulation

The classic 2/3 PHx model was established as previously described.⁴¹ Briefly, the mice were anesthetized. A midline abdominal incision was performed to expose the abdominal cavity. The left lateral and median hepatic lobes were ligated and sectioned off. For acute liver intoxication by CCl₄, the mice were injected intraperitoneally with a dose of 10% CCl₄ or sterile olive oil at 10 μL/g once.^{42,43} LPS (4 mg/kg) was injected intraperitoneally immediately after 2/3 PHx for additional stimulation. Liver samples were collected from the remaining lobes and then either were snap-frozen in liquid nitrogen and stored at -80°C or fixed in 4% paraformaldehyde.

Histologic Assessment, Immunohistochemistry, and Immunofluorescence

Liver samples were embedded in paraffin and cut into 4-μm sections. The slices were processed routinely with H&E staining. For immunostaining, heat-mediated antigen retrieval was performed after dewaxing and rehydration of the slices. Endogenous peroxidase was quenched with 3% H₂O₂. The slices were blocked with normal goat serum and

Figure 11. Response of hepatocytes with intervened GMFB expression to IL6 stimulation and level of the STAT3/cyclin D1 axis in liver of PHx and LPS-treated mice. Representative immunofluorescence staining images in EdU staining (red) L02 cells (hepatocyte cell line) transfected with (A) *GMFB* siRNAs or control siRNA (normal control), and (B) with *GMFB* over-expression plasmid (GMFB) or control plasmid (vehicle) and percentage of EdU-positive-staining cells. Data represent the average of 3 independent experiments. n > 300 cells for each group. (A) One-way analysis of variance, (B) 2-tailed *t* test. Flow cytometry analyses showing the percentage of cells at cell-cycle phases G0/G1, S, or G2/M of L02 cells transfected with (C) siRNAs or NC, and (D) with GMFB or vehicle. Data represent the average of 3 independent experiments. n > 10⁶ cells for each group. (C) One-way analysis of variance, (D) 2-tailed *t* test. (E and F) Protein levels of GMFB, CCND1, p-STAT3, and STAT3 in L02 cells transfected with (E) siRNAs or NC, and with (F) GMFB or vehicle. (E) One-way analysis of variance, (F) 2-tailed *t* test. Data represent the average of 3 independent experiments. Flow cytometry analyses showing the percentage of EdU-positive-staining L02 cells transfected with (G) siRNAs or NC, and with (H) GMFB or vehicle and treated with IL6 or bovine serum albumin (BSA). Data represent the average of 3 independent experiments. n > 10⁶ cells for each group. (G) One-way analysis of variance; (H) 2-tailed *t* test, **P* < .05, ****P* < .001, vs NC or vehicle groups. (I) Co-immunoprecipitation analysis of L02 cells treated with IL6 showing if there was any interaction between STAT3 and GMFB. Data represent the average of 3 independent experiments. (J) Protein levels of GMFB, CCND1, p-STAT3, and STAT3 in liver from *Gmfb* KO and WT mice after PHx and with an immediate subsequent LPS injection. n = 4 mice for each group. Two-tailed *t* test, **P* < .05, ***P* < .01, ****P* < .001, vs WT controls. CCND1, cyclin D1; GAPDH, glyceraldehyde-3-phosphate dehydrogenase.

incubated overnight in primary antibodies. For immunohistochemistry, the primary antibodies included anti-MKI67, anti-proliferating cell nuclear antigen, anti-IL6, and anti-YAP1. The samples then were incubated with peroxidase-conjugated anti-rat or anti-rabbit antibodies for 1 hour. Chromogenic detection was performed with a diaminobenzidine histochemistry kit. Immunoreactivity was visualized using a brown horseradish peroxide substrate. For immunofluorescence, the primary antibodies included anti-STAT3, anti-GMFB, anti-HNF4 α , anti-F4/80, and anti-desmin. The secondary antibodies were goat anti-rabbit IgG (H+L), fluorescein isothiocyanate (FITC) conjugate, goat anti-rabbit IgG (H+L), and Cy3 conjugate. For oil red O staining, liver tissues were fixed in 4% paraformaldehyde and then were dehydrated in 30% sucrose overnight. The frozen samples were cut into 10- μ m sections, and then were washed with phosphate-buffered saline (PBS), rinsed with 60% isopropyl alcohol, and stained with freshly prepared oil red O working solution. Then, the sections were rinsed with 60% isopropyl alcohol, stained with alum hematoxylin, and, finally, were mounted in aqueous mountant.

Western Blot

Liver samples were homogenized within RIPA buffer. Total protein in the supernatant was collected by centrifuge at $13,000 \times g$ for 20 minutes at 4°C. The lysate then was diluted with $5 \times$ sodium dodecyl sulfate loading buffer and boiled and stored at -80°C. Western blot was performed. The primary antibodies included anti-GMFB, anti-STAT3, anti-p-STAT3 (Y705), anti-histone H3, anti-cyclin D1, anti-JAK2, anti-p-JAK2, anti-CDK4, anti-CDK2, anti-histone H3 serine 10 phosphorylation, anti-glyceraldehyde-3-phosphate dehydrogenase, anti-acetyl-coenzyme A carboxylase α , anti-glycerol-3-phosphate acyltransferase, mitochondrial, anti-peroxisome proliferator activated receptor α , anti-IL1B, anti-TNF, anti-IL6, anti-YAP1, anti-p-YAP, and anti- β -actin. For identification of GMFB separately in cytoplasm and nucleus, the homogenized samples were treated with a nuclear protein extraction kit. The cytoplasmic and nuclear components then were subjected to Western blot. Glyceraldehyde-3-phosphate dehydrogenase and histone H3 were used as markers for cytoplasm and the nucleus, respectively.

qPCR, RNA-Seq, and Bioinformatics Analysis

For qPCR, total RNA was extracted using an RNAiso Plus kit (TAKARA BIO) and complementary DNA was generated using a PrimeScript reverse transcription kit (TAKARA BIO). The primer sequences used for qPCR are listed in [Supplementary Table 5](#). qPCR was performed in quadruplicate using SYBR Premix Ex Taq (TAKARA BIO). Fold change was determined using the $2^{-\Delta\Delta\text{cycle threshold}}$ method. For RNA-seq, total RNA was extracted using TRIzol reagent (Thermo Fisher). A double-ended library was made and sequencing was performed on an Illumina NovaSeq 6000 (Illumina) platform with 150-bp paired-end reads in Novogene Co. Ltd. (Beijing, China). Reads were mapped to a reference genome sequence (GRCm38/mm10) using HisAT2

software (2.0.5; R package). Differentially expressed genes were defined by fold change and statistical significance. Functional profiling was performed using Gene Ontology,⁴⁴ Kyoto Encyclopedia of Genes and Genomes databases,⁴⁵ and gene set enrichment analysis.⁴⁶

Cell Culture and Treatment

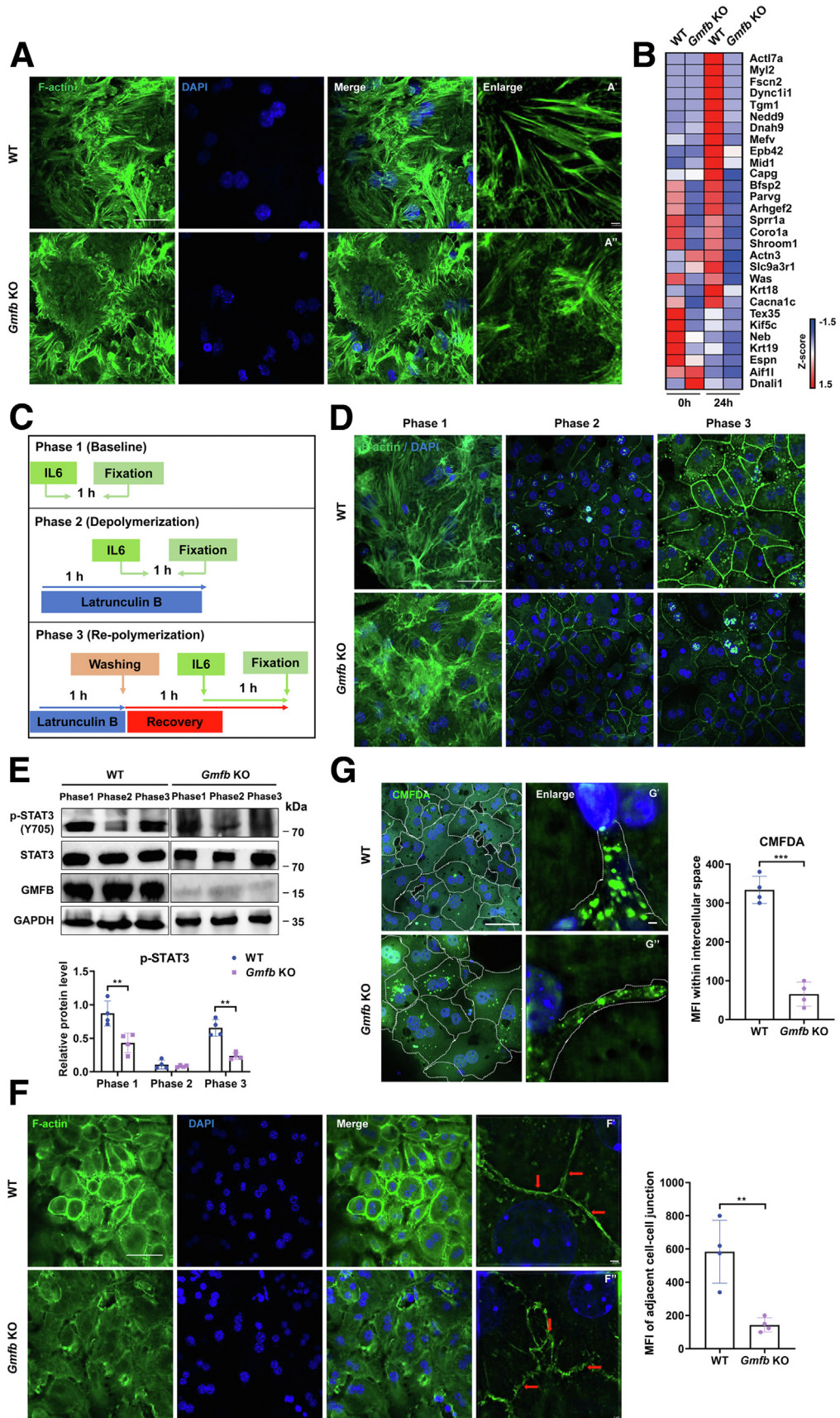
Human hepatocyte cell line L02 cells were cultured in low-glucose Dulbecco's modified Eagle medium (DMEM) supplemented with 10% fetal bovine serum (FBS). Human GMFB siRNA, overexpression plasmid, and the controls were purchased from Ribo Biosciences. siRNAs (50 nmol/L) were transfected using Lipofectamine 3000 (Invitrogen) reagent following the manufacturer's instructions. For IL6 stimulation,⁴⁷ L02 cells were starved for 2 hours with serum-free DMEM and then cultured with human recombinant IL6 (15 ng/mL) for 24 hours. 5-ethynyl-2'-deoxyuridine (EdU) staining was performed using BeyoClick EdU cell proliferation kit (Beyotime) with Alexa Fluor 594. Fresh DMEM with EdU at a final concentration of 10 μ mol/L was used to incubate the cells for 2 hours. Then, the cells were washed and fixed in 4% paraformaldehyde. The cell nucleus was stained with 4',6-diamidino-2-phenylindole (DAPI).

Flow Cytometry Analysis

For cell-cycle analysis, L02 cells were harvested, washed with PBS, and fixed with cold 70% ethanol. After washing with PBS, 50 μ L RNase A solution (100 μ g/mL) was added and the cells were incubated for 30 minutes at 37°C. Then, 500 μ L propidium iodide solution (50 μ g/mL) was added per 10^6 cells and the cells were incubated for 30 minutes at room temperature. The samples then were analyzed using a flow cytometer. The percentage of cells at different phases of the cell cycle was analyzed using FlowJo software (7.6; BD Biosciences). For counting EdU-stained cells, EdU staining was performed using the BeyoClick EdU cell proliferation kit with Alexa Fluor 594 as described earlier. Then, the cells were harvested and fixed in 4% formaldehyde for 15 minutes at room temperature. The cells were incubated with 0.3% Triton X-100 (Beyotime) for 10 minutes, washed, and incubated with Beyotime's staining solution for EdU click reaction. The cell nucleus was stained with DAPI. Then, the samples were analyzed using a flow cytometer.

Co-immunoprecipitation Analysis

Co-immunoprecipitation was performed with a immunoprecipitation/Co-immunoprecipitation kit according to the manufacturer's instructions. L02 cells were starved for 6 hours and then cultured with IL6 (15 ng/mL) for another 24 hours. The cells were harvested using lysis buffer supplemented with phenylmethylsulfonyl fluoride (1 mmol/l). The supernatant was precleared with protein A/G-agarose beads for 1 hour with agitation at 4°C, followed by incubation with primary antibodies and general agitation at 4°C overnight and then with protein A/G-agarose beads for another 3 hours. After washing 4 times with wash buffer, the pellets were mixed with $1 \times$ sodium dodecyl sulfate buffer, boiled



for 5 minutes, and then processed for Western blot. Primary antibodies used for immunoprecipitation were anti-STAT3, anti-GMFB, and anti-IgG.

Isolation of Primary Hepatocytes and Treatment With Oleic Acid

All the mice were maintained with normal chow diet. Primary hepatocytes were isolated using 2-step collagenase perfusion.⁴⁸ Briefly, mice were anesthetized and had their abdominal cavity exposed. The livers were perfused in situ with Ca^{2+} , Mg^{2+} free D-Hanks' (Genom) balanced solution containing HEPES (25 mmol/L), glucose (1 g/L), ethylene glycol-bis(β -aminoethyl ether)-*N,N,N',N'*-tetraacetic acid/EDTA (0.5 mmol/L), and penicillin-streptomycin (1% v/v), and then with Hanks' balanced solution containing collagenase (type II, 20 U/mL), HEPES (15 mmol/L), and penicillin-streptomycin (1% v/v). Dissociated liver was passed through a 70- μm cell strainer and the hepatocytes were enriched by low-speed centrifugation ($50 \times g$ for 3 minutes) in Williams' E medium. Only samples with cell viability >90% were used for culture. Hepatocytes were inoculated into collagen I-coated 6-well plates (5×10^5 /well) in Williams' E medium with 10% FBS, and allowed to establish a monolayer for 2 hours. Then, the medium was replaced with fresh supplemented medium without FBS containing epidermal growth factor (5 ng/mL), insulin (0.2 U/mL), and dexamethasone (100 nmol/L). Hepatocytes were processed further to morphology or metabolite excretion assessment at 24, 48, or 72 hours after seeding as described in the Figure 5 and 12 legends. Oleic acid at 0.3 mmol/L was used for hepatocyte steatosis modeling. After 24 hours of cell culture, the medium was collected and cells were harvested for further assays.

Isolation of Kupffer Cells and Treatment With LPS

Kupffer cells were separated as previously described.⁴⁹ Nonparenchymal liver cells were enriched by centrifugation at $500 \times g$ for 5 minutes. The sediment cells were resuspended with 25% Percoll in stock isotonic solution in 0.15 mol/L NaCl. The cell suspension was applied between 2 layers of solution, a lower layer of 50% Percoll, and an upper layer of D-Hanks buffer, and centrifuged at $900 \times g$ for 20 minutes. Then, the cells in the third layer were collected and washed with PBS twice. The enriched Kupffer

cells then were cultured in RPMI 1640 medium containing 10% FBS for 24 hours. The RPMI 1640 medium was changed and Kupffer cells were treated with LPS (20 $\mu\text{g}/\text{mL}$) for 6 hours. The inflammatory cytokines (IL6, TNF, and IL1 β) in the supernatant of Kupffer cells were detected using an enzyme-linked immunosorbent assay.

Isolation of HSCs

HSCs were isolated from the liver nonparenchymal cells basically according to a previous publication.⁵⁰ Nonparenchymal cells were enriched by centrifugation at $350 \times g$ for 10 minutes. The sediment cells were resuspended in 8 mL RPMI 1640 medium and were applied on 3 layers of solution, including a lower layer of 50% Percoll, a middle layer of 35% Percoll, and an upper layer of $1 \times \text{PBS}$, and were centrifuged at $900 \times g$ for 30 minutes. Then, cells between the middle and upper layers were collected and washed with RPMI 1640 medium at $900 \times g$ for 10 minutes twice. The enriched cells then were cultured in RPMI 1640 medium containing 10% FBS and harvested for further assays.

Phalloidin-FITC Staining of F-Actin and Excretion of CMFDA in Primary Hepatocytes

To image F-actin in cells, the cultured primary hepatocytes were fixed and stained with phalloidin-FITC (5 $\mu\text{g}/\text{mL}$). The cell nucleus then was stained with DAPI. For the hepatocyte excretion test, primary hepatocytes grown on coverslips in 24-well plates were cultured for 24 hours. CMFDA probe working solution (5 $\mu\text{mol}/\text{L}$) was added into the cell culture wells, and hepatocytes were incubated for 45 minutes at 37°C. Then, cells were washed with PBS and fixed with 4% paraformaldehyde. Antifluorescence quencher was used to seal coverslips. CMFDA in hepatocyte cytosol and the intercellular space between adjacent cells were imaged.

Imaging Assessment

Morphologic sections were imaged by optical microscopy (BX63; Olympus), or laser scanning confocal microscopy (LSM980; Zeiss), or transmission electron microscopy (H-7500; Hitachi). Super-resolution microscopy (N-SIM-STORM; Nikon) was used for location of CMFDA and discernment of actin filaments. Quantification of fluorescent

Figure 12. GMFB modulates actin-filament organization, which facilitates hepatocyte response of STAT3 activation to IL6 treatment. (A) Representative immunofluorescent images in 72 hours after seeding primary hepatocytes with F-actin stained (phalloidin, green). Scale bars: 50 μm (A), 2 μm (A', A''). (B) Heatmap showing the gene expression values (fragments per kilobase of transcript per million mapped reads) of indicated genes (RNA-seq) associated with actin-filament organization in comparison with WT and *Gmfb* KO groups. $n = 2$ mice for each group. (C) Schematic for treatment 48 hours after seeding of primary hepatocytes with IL6 and latrunculin B for actin-filament polymerization assay and (D) representative immunofluorescent images in the cells with F-actin stained (phalloidin, green). Scale bar: 50 μm . (E) Protein levels of p-STAT3, STAT3, and GMFB in treated hepatocytes for which the treatment is illustrated in panel C from *Gmfb* KO and WT mice. $n = 4$ mice for each group. Two-tailed *t* test, $**P < .01$, vs WT controls. (F) Representative immunofluorescent images in 24 hours after seeding primary hepatocytes with F-actin stained (phalloidin, green). Red arrows indicate actin filaments between adjacent hepatocytes. Scale bars: 50 μm (F), 2 μm (F', F''). The mean fluorescence intensity (MFI) of the adjacent cellular junction was quantified from $n > 200$ cells for each group. Two-tailed *t* test, $**P < .01$, vs WT hepatocytes. (G) Representative fluorescent images of 24 hours after seeding primary hepatocytes incubated with CMFDA (green) for 45 minutes and then washed off. Individual cell boundaries are outlined with a dotted line. Scale bars: 50 μm (G), 2 μm (G', G''). The MFI of CMFDA within the intercellular space was quantified from $n > 200$ cells for each group. Two-tailed *t* test, $***P < .001$, vs WT hepatocytes. Data represent 4 independent experiments. GAPDH, glyceraldehyde-3-phosphate dehydrogenase.

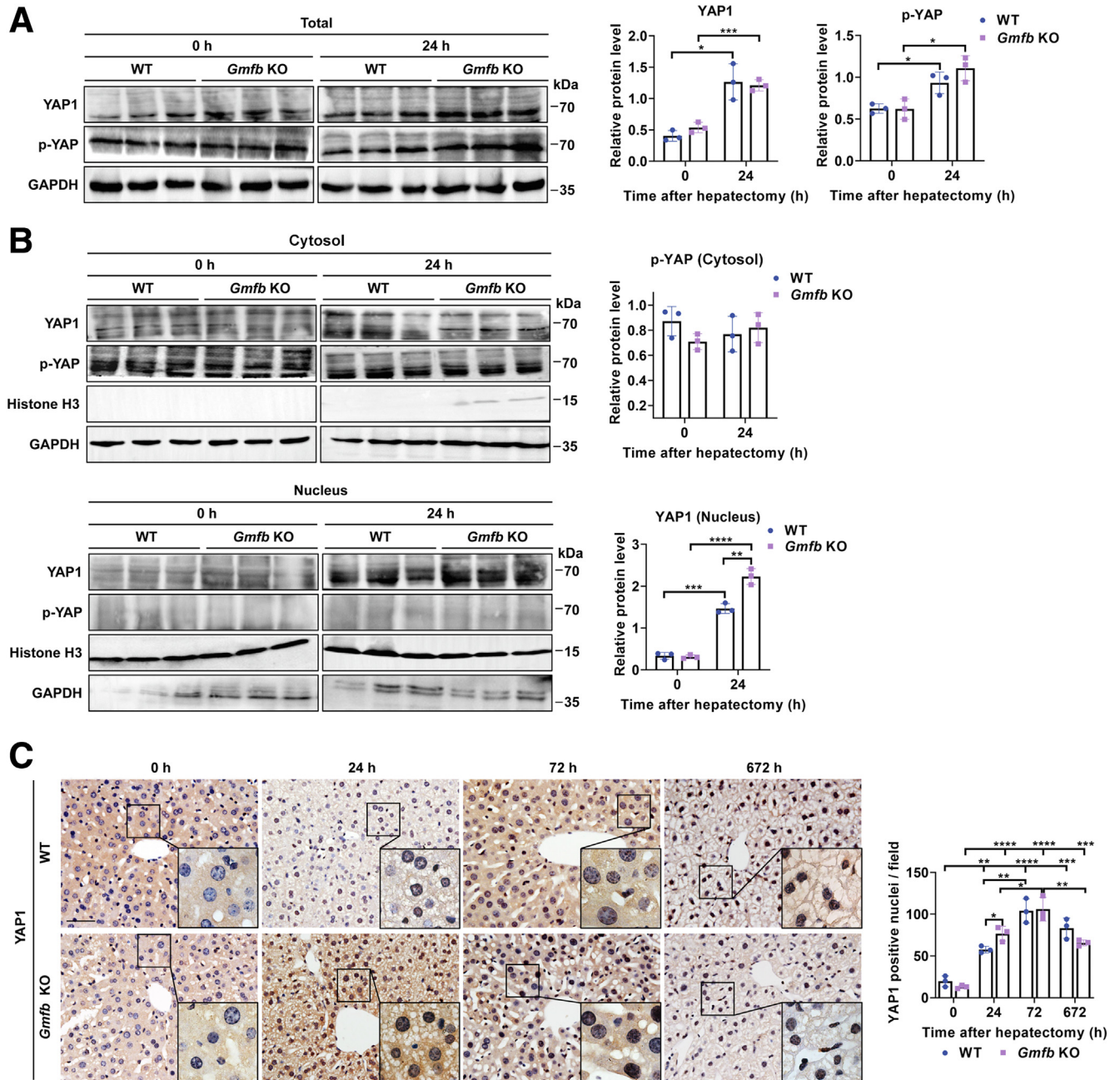


Figure 13. Protein levels of YAP1 and p-YAP in liver from mice after PHx. (A and B) Protein levels of YAP1 and p-YAP in liver from *Gmfb* KO and WT groups at the indicated time points after PHx. (A) Total protein; (B) Cytosol protein and nucleus protein. n = 3 mice for each group. (C) Representative immunochemical images in anti-YAP1–stained liver sections from *Gmfb* KO and WT groups (scale bar: 50 μm) and quantification of numbers per field of YAP1-positive staining nuclei in liver slices. n = 3 mice for each group. Two-tailed *t* test, **P* < .05, ***P* < .01, ****P* < .001, and *****P* < .0001, vs WT controls. GAPDH, glyceraldehyde-3-phosphate dehydrogenase.

or optical objects of interest (OIs) was conducted using Image Pro Plus 6.0 (Media Cybernetics). Sample slices were scanned into digitized images. Then, to determine the area of OI in tissue sections, 10–15 image tiles were selected randomly in the assessment images for each sample slice, and OI was identified manually and its morphometric area was calculated using the software tool. Then, the ratio of total area of OIs to the area of the entire image tile was

considered as the OI value. To determine the area of OI in cell culture images, the area of entire cellular images was used as the denominator, the ratio then was divided further by the number of total cells within the same image tile and, finally, was considered as the OI value; the rest of the protocols were similar to the tissue section protocols. To determine the number of OI-positive-labeling cells, the number of cells stained with OI was calculated and then

divided by the number of all target cells within the same image tile, the ratio was considered the OI value. To determine cell size, 10 image tiles were selected randomly for each sample slice. In each tile, every cell size was measured manually using the Zeiss software ZEN 3.2 and counted, the average cell size within each tile was used as the cell size for the tile and the average cell size of all the image tiles was used as the cell size for the sample slice.

Statistical Analysis

Statistical analyses were performed using GraphPad Prism 8.3.0 or R software 4.0.4 (The R Foundation). Further details are available in the Figure legends. Unless stated otherwise, all experiments were repeated independently at least 3 times. All bar and line plots show data as means \pm SEM. A 2-sided *P* value of less than .05 was considered statistically significant.

All authors had access to the study data and reviewed and approved the final manuscript. All the present data, analytical methods, and information on study materials will be available for any scientific researcher who requires the data and contacts the authors (G.Y., W.Z., or Y.W.).

References

1. Michalopoulos GK. Hepatostat: liver regeneration and normal liver tissue maintenance. *Hepatology* 2017; 65:1384–1392.
2. Forbes SJ, Newsome PN. Liver regeneration - mechanisms and models to clinical application. *Nat Rev Gastroenterol Hepatol* 2016;13:473–485.
3. Michalopoulos GK, Bhushan B. Liver regeneration: biological and pathological mechanisms and implications. *Nat Rev Gastroenterol Hepatol* 2021;18:40–55.
4. Campana L, Esser H, Huch M, Forbes S. Liver regeneration and inflammation: from fundamental science to clinical applications. *Nat Rev Mol Cell Biol* 2021; 22:608–624.
5. Yang L, Magness ST, Bataller R, Rippe RA, Brenner DA. NF- κ B activation in Kupffer cells after partial hepatectomy. *Am J Physiol Gastrointest Liver Physiol* 2005; 289:G530–G538.
6. Barbier L, Ferhat M, Salame E, Robin A, Herbelin A, Gombert JM, Silvain C, Barbarin A. Interleukin-1 family cytokines: keystones in liver inflammatory diseases. *Front Immunol* 2019;10:2014.
7. Taub R. Liver regeneration: from myth to mechanism. *Nat Rev Mol Cell Biol* 2004;5:836–847.
8. Fazel Modares N, Polz R, Haghghi F, Lamertz L, Behnke K, Zhuang Y, Kordes C, Haussinger D, Sorg UR, Pfeffer K, Floss DM, Moll JM, Piekorz RP, Ahmadian MR, Lang PA, Scheller J. IL-6 trans-signaling controls liver regeneration after partial hepatectomy. *Hepatology* 2019;70:2075–2091.
9. Goode BL, Sweeney MO, Eskin JA. GMF as an actin network remodeling factor. *Trends Cell Biol* 2018; 28:749–760.
10. Haynes EM, Asokan SB, King SJ, Johnson HE, Haugh JM, Bear JE. GMFBeta controls branched actin content and lamellipodial retraction in fibroblasts. *J Cell Biol* 2015;209:803–812.
11. Poukkula M, Hakala M, Pentimikko N, Sweeney MO, Jansen S, Mattila J, Hietakangas V, Goode BL, Lappalainen P. GMF promotes leading-edge dynamics and collective cell migration in vivo. *Curr Biol* 2014; 24:2533–2540.
12. Lim R, Mitsunobu K, Li WK. Maturation-stimulating effect of brain extract and dibutyryl cyclic AMP on dissociated embryonic brain cells in culture. *Exp Eye Res* 1973; 79:243–246.
13. Zaheer A, Zaheer S, Thangavel R, Wu Y, Sahu SK, Yang B. Glia maturation factor modulates beta-amyloid-induced glial activation, inflammatory cytokine/chemokine production and neuronal damage. *Brain Res* 2008; 1208:192–203.
14. Yin G, Du M, Li R, Li K, Huang X, Duan D, Ai X, Yao F, Zhang L, Hu Z, Wu B. Glia maturation factor beta is required for reactive gliosis after traumatic brain injury in zebrafish. *Exp Neurol* 2018;305:129–138.
15. Uhlen M, Fagerberg L, Hallstrom BM, Lindskog C, Oksvold P, Mardinoglu A, Sivertsson A, Kampf C, Sjostedt E, Asplund A, Olsson I, Edlund K, Lundberg E, Navani S, Szgyarto CA, Odeberg J, Djureinovic D, Takanen JO, Hober S, Alm T, Edqvist PH, Berling H, Tegel H, Mulder J, Rockberg J, Nilsson P, Schwenk JM, Hamsten M, von Feilitzen K, Forsberg M, Persson L, Johansson F, Zwahlen M, von Heijne G, Nielsen J, Ponten F. Proteomics. Tissue-based map of the human proteome. *Science* 2015;347:1260419.
16. Jiang Y, Sun A, Zhao Y, Ying W, Sun H, Yang X, Xing B, Sun W, Ren L, Hu B, Li C, Zhang L, Qin G, Zhang M, Chen N, Zhang M, Huang Y, Zhou J, Zhao Y, Liu M, Zhu X, Qiu Y, Sun Y, Huang C, Yan M, Wang M, Liu W, Tian F, Xu H, Zhou J, Wu Z, Shi T, Zhu W, Qin J, Xie L, Fan J, Qian X, He F. Chinese Human Proteome Project (CNHPP) Consortium. Proteomics identifies new therapeutic targets of early-stage hepatocellular carcinoma. *Nature* 2019;567:257–261.
17. Sun W, Hu C, Wang T, Wang J, Zhang J, Gao F, Ou Q, Tian H, Jin C, Xu J, Zhang J, Xu GT, Lu L. Glia maturation factor beta as a novel biomarker and therapeutic target for hepatocellular carcinoma. *Front Oncol* 2021;11:744331.
18. Moylan CA, Pang H, Dellinger A, Suzuki A, Garrett ME, Guy CD, Murphy SK, Ashley-Koch AE, Choi SS, Michelotti GA, Hampton DD, Chen Y, Tillmann HL, Hauser MA, Abdelmalek MF, Diehl AM. Hepatic gene expression profiles differentiate presymptomatic patients with mild versus severe nonalcoholic fatty liver disease. *Hepatology* 2014;59:471–482.
19. Ahrens M, Ammerpohl O, von Schonfels W, Kolarova J, Bens S, Itzel T, Teufel A, Herrmann A, Brosch M, Hinrichsen H, Erhart W, Egberts J, Sipos B, Schreiber S, Hasler R, Stickel F, Becker T, Krawczak M, Rocken C, Siebert R, Schafmayer C, Hampe J. DNA methylation analysis in nonalcoholic fatty liver disease suggests distinct disease-specific and remodeling signatures after bariatric surgery. *Cell Metab* 2013;18:296–302.
20. Nissim O, Melis M, Diaz G, Kleiner DE, Tice A, Fantola G, Zamboni F, Mishra L, Farci P. Liver regeneration

- signature in hepatitis B virus (HBV)-associated acute liver failure identified by gene expression profiling. *PLoS One* 2012;7:e49611.
21. Affo S, Dominguez M, Lozano JJ, Sancho-Bru P, Rodrigo-Torres D, Morales-Ibanez O, Moreno M, Millan C, Loaeza-del-Castillo A, Altamirano J, Garcia-Pagan JC, Arroyo V, Gines P, Caballeria J, Schwabe RF, Bataller R. Transcriptome analysis identifies TNF superfamily receptors as potential therapeutic targets in alcoholic hepatitis. *Gut* 2013;62:452–460.
 22. Higgins GM, Anderson RM. Experimental pathology of the liver. I. Restoration of the liver of the white rat following partial surgical removal. *Arch Pathol* 1931;12:186–202.
 23. Michalopoulos GK, DeFrances MC. Liver regeneration. *Science* 1997;276:60–66.
 24. Cressman DE, Greenbaum LE, DeAngelis RA, Ciliberto G, Furth EE, Poli V, Taub R. Liver failure and defective hepatocyte regeneration in interleukin-6-deficient mice. *Science* 1996;274:1379–1383.
 25. Gao B, Wang H, Lafdil F, Feng D. STAT proteins - key regulators of anti-viral responses, inflammation, and tumorigenesis in the liver. *J Hepatol* 2012;57:430–441.
 26. Nelsen CJ, Rickheim DG, Timchenko NA, Stanley MW, Albrecht JH. Transient expression of cyclin D1 is sufficient to promote hepatocyte replication and liver growth in vivo. *Cancer Res* 2001;61:8564–8568.
 27. Cressman DE, Diamond RH, Taub R. Rapid activation of the Stat3 transcription complex in liver regeneration. *Hepatology* 1995;21:1443–1449.
 28. Li N, Hua J. Immune cells in liver regeneration. *Oncotarget* 2017;8:3628–3639.
 29. Ait Ahmed Y, Fu Y, Rodrigues RM, He Y, Guan Y, Guillot A, Ren R, Feng D, Hidalgo J, Ju C, Lafdil F, Gao B. Kupffer cell restoration after partial hepatectomy is mainly driven by local cell proliferation in IL-6-dependent autocrine and paracrine manners. *Cell Mol Immunol* 2021;18:2165–2176.
 30. Corry J, Mott HR, Owen D. Activation of STAT transcription factors by the Rho-family GTPases. *Biochem Soc Trans* 2020;48:2213–2227.
 31. Pelletier S, Duhamel F, Coulombe P, Popoff MR, Meloche S. Rho family GTPases are required for activation of Jak/STAT signaling by G protein-coupled receptors. *Mol Cell Biol* 2003;23:1316–1333.
 32. Wang Y, Toh YC, Li Q, Nugraha B, Zheng B, Lu TB, Gao Y, Ng MM, Yu H. Mechanical compaction directly modulates the dynamics of bile canaliculi formation. *Integr Biol (Camb)* 2013;5:390–401.
 33. Russell JO, Camargo FD. Hippo signalling in the liver: role in development, regeneration and disease. *Nat Rev Gastroenterol Hepatol* 2022;19:297–312.
 34. Inagaki M, Aoyama M, Sobue K, Yamamoto N, Morishima T, Moriyama A, Katsuya H, Asai K. Sensitive immunoassays for human and rat GMFB and GMFG, tissue distribution and age-related changes. *Biochim Biophys Acta* 2004;1670:208–216.
 35. Karin M, Clevers H. Reparative inflammation takes charge of tissue regeneration. *Nature* 2016;529:307–315.
 36. Li W, Liang X, Kellendonk C, Poli V, Taub R. STAT3 contributes to the mitogenic response of hepatocytes during liver regeneration. *J Biol Chem* 2002;277:28411–28417.
 37. Xu L, Hui AY, Albanis E, Arthur MJ, O'Byrne SM, Blaner WS, Mukherjee P, Friedman SL, Eng FJ. Human hepatic stellate cell lines, LX-1 and LX-2: new tools for analysis of hepatic fibrosis. *Gut* 2005;54:142–151.
 38. El Taghdouini A, Sorensen AL, Reiner AH, Coll M, Verhulst S, Mannaerts I, Oie CI, Smedsrod B, Najimi M, Sokal E, Luttun A, Sancho-Bru P, Collas P, van Grunsven LA. Genome-wide analysis of DNA methylation and gene expression patterns in purified, uncultured human liver cells and activated hepatic stellate cells. *Oncotarget* 2015;6:26729–26745.
 39. Kitto LJ, Henderson NC. Hepatic stellate cell regulation of liver regeneration and repair. *Hepatol Commun* 2021;5:358–370.
 40. Klepeisz P, Sagmeister S, Haudek-Prinz V, Pichlbauer M, Grasl-Kraupp B, Gerner C. Phenobarbital induces alterations in the proteome of hepatocytes and mesenchymal cells of rat livers. *PLoS One* 2013;8:e76137.
 41. Mitchell C, Willenbring H. A reproducible and well-tolerated method for 2/3 partial hepatectomy in mice. *Nat Protoc* 2008;3:1167–1170.
 42. Kovalovich K, DeAngelis RA, Li W, Furth EE, Ciliberto G, Taub R. Increased toxin-induced liver injury and fibrosis in interleukin-6-deficient mice. *Hepatology* 2000;31:149–159.
 43. Bansal MB, Kovalovich K, Gupta R, Li W, Agarwal A, Radbill B, Alvarez CE, Safadi R, Fiel MI, Friedman SL, Taub RA. Interleukin-6 protects hepatocytes from CCl4-mediated necrosis and apoptosis in mice by reducing MMP-2 expression. *J Hepatol* 2005;42:548–556.
 44. Ashburner M, Ball CA, Blake JA, Botstein D, Butler H, Cherry JM, Davis AP, Dolinski K, Dwight SS, Eppig JT, Harris MA, Hill DP, Issel-Tarver L, Kasarskis A, Lewis S, Matese JC, Richardson JE, Ringwald M, Rubin GM, Sherlock G. Gene ontology: tool for the unification of biology. The Gene Ontology Consortium. *Nat Genet* 2000;25:25–29.
 45. Kanehisa M, Goto S. KEGG: Kyoto Encyclopedia of Genes and Genomes. *Nucleic Acids Res* 2000;28:27–30.
 46. Mootha VK, Lindgren CM, Eriksson KF, Subramanian A, Sihag S, Lehar J, Puigserver P, Carlsson E, Ridderstrale M, Laurila E, Houstis N, Daly MJ, Patterson N, Mesirov JP, Golub TR, Tamayo P, Spiegelman B, Lander ES, Hirschhorn JN, Altshuler D, Groop LC. PGC-1alpha-responsive genes involved in oxidative phosphorylation are coordinately down-regulated in human diabetes. *Nat Genet* 2003;34:267–273.
 47. Suh HN, Lee SH, Lee MY, Lee YJ, Lee JH, Han HJ. Role of interleukin-6 in the control of DNA synthesis of hepatocytes: involvement of PKC, p44/42 MAPKs, and PPARdelta. *Cell Physiol Biochem* 2008;22:673–684.
 48. Shen L, Hillebrand A, Wang DQ, Liu M. Isolation and primary culture of rat hepatic cells. *J Vis Exp* 2012;64:3917.
 49. Froh M, Konno A, Thurman RG. Isolation of liver Kupffer cells. *Curr Protoc Toxicol* 2003:Chapter 14:Unit14.4.

50. Vrochides D, Papanikolaou V, Pertoft H, Antoniadis AA, Heldin P. Biosynthesis and degradation of hyaluronan by nonparenchymal liver cells during liver regeneration. *Hepatology* 1996;23:1650–1655.

Received February 13, 2022. Accepted July 25, 2022.

Correspondence

Address correspondence to: Yan Wang, MD, PhD, Biomedical Research Center, Southern Medical University, No 1023 Sha Tai Nan Avenue, Guangzhou 510515, China. e-mail: Yanwang@smu.edu.cn; fax: (86) 20-6164-7396.

Acknowledgments

The authors would like to thank Dr Tianrong Xun (Southern Medical University, Guangzhou, China) for kindly providing L02 cells; Ms Ke Li (Southern Medical University Nanfang Hospital, Guangzhou, China) for flow cytometry; and Dr Zhitao Zhou and Dr Yanmeng Lu (Southern Medical University Biomedical Research Center, Guangzhou, China) for transmission electron microscopy.

CRediT Authorship Contributions

Guo Yin (Data curation: Lead; Formal analysis: Equal; Funding acquisition: Equal; Methodology: Equal; Validation: Lead; Writing – original draft: Equal)

Weilan Zeng (Data curation: Lead; Formal analysis: Lead; Investigation: Lead; Software: Lead; Validation: Equal; Visualization: Lead; Writing – review & editing: Equal)

Rong Li (Formal analysis: Equal; Investigation: Supporting; Project administration: Supporting; Software: Equal; Writing – original draft: Equal)

Manman Zeng (Data curation: Supporting; Methodology: Supporting; Resources: Supporting; Validation: Supporting)

Ronghua Chen (Methodology: Supporting; Project administration: Supporting; Resources: Supporting)

Yaxue Liu (Data curation: Supporting; Formal analysis: Supporting; Investigation: Supporting; Project administration: Supporting)

Ronglong Jiang (Conceptualization: Supporting; Funding acquisition: Supporting; Investigation: Supporting; Project administration: Supporting; Resources: Supporting)

Yan Wang, MD, PhD (Conceptualization: Lead; Formal analysis: Equal; Funding acquisition: Lead; Methodology: Equal; Project administration: Lead; Resources: Lead; Supervision: Lead; Visualization: Equal; Writing – original draft: Lead; Writing – review & editing: Lead)

Ethics statement

Animal experiments were approved by the Ethical Committee for Animal Research of Southern Medical University and were conducted based on the state guidelines from the Ministry of Science and Technology of China.

Conflicts of interest

The authors disclose no conflicts.

Funding

This study was supported in part by the National Natural Science Foundation of China grants 82070589 and 81670522, Sanming Project of Medicine in Shenzhen grant SZSM201911001, and Guangzhou Science and Technology Plan Project grant 2022-01-01-11-3028-0062 (Y.W.); and by the National Natural Science Foundation of China grant 81901263 (G.Y.).

Data transparency

All the present data, analytical methods, and information on study materials will be available for any scientific researcher who requires and contacts the authors (G.Y., W.Z., or Y.W.). Transcriptome profiling data generated in this study can be downloaded at the repository URL <https://www.ncbi.nlm.nih.gov/sra> with data accession number PRJNA805036 or SRP359344.